ASTROBIOLOGY
Volume 20, Number 8, 2020

DOI: 10.1089/ast.2019.2132

Fluvial Regimes, Morphometry, and Age of Jezero Crater Paleolake Inlet Valleys and Their Exobiological Significance for the 2020 Rover Mission Landing Site

Nicolas Mangold,[1] Gilles Dromart,[2] Veronique Ansan,[1] Francesco Salese,[3,4] Maarten G. Kleinhans,[3] Marion Massé,[1] Cathy Quantin-Nataf,[2] and Kathryn M. Stack[5]

Abstract

Jezero crater has been selected as the landing site for the Mars 2020 Perseverance rover, because it contains a paleolake with two fan-deltas, inlet and outlet valleys. Using the data from the High Resolution Stereo Camera (HRSC) and the High Resolution Imaging Science Experiment (HiRISE), we conducted a quantitative geomorphological study of the inlet valleys of the Jezero paleolake. Results show that the strongest erosion is related to a network of deep valleys that cut into the highland bedrock well upstream of the Jezero crater and likely formed before the formation of the regional olivine-rich unit. In contrast, the lower sections of valleys display poor bedrock erosion and a lack of tributaries but are characterized by the presence of pristine landforms interpreted as fluvial bars from preserved channels, the discharge rates of which have been estimated at 10^3–10^4 m^3s^{-1}. The valleys' lower sections postdate the olivine-rich unit, are linked directly to the fan-deltas, and are thus formed in an energetic, late stage of activity. Although a Late Noachian age for the fan-deltas' formation is not excluded based on crosscutting relationships and crater counts, this indicates evidence of a Hesperian age with significant implications for exobiology. Key Words: Mars—Perseverance rover—Landing site—HiRISE—HRSC—Fluvial landforms. Astrobiology 20, 994–1013.

1. Introduction

Jezero crater has been interpreted as a paleolake due to the presence of two inlet fluvial valleys linked to two depositional fans and one outlet valley on the other side of the crater (Fassett and Head, 2005; Schon *et al.*, 2012; Goudge *et al.*, 2015). The Jezero crater (18.2°N, 77.6°E) is located east of Nili Fossae, west of the Isidis Planitia, and north of Syrtis Major Planum volcanic province, in a region dominated by a mafic ancient crust broadly associated with clay minerals that are indicative of a substantial aqueous alteration (*e.g.*, Poulet *et al.*, 2005; Mangold *et al.*, 2007; Mustard *et al.*, 2007, 2009; Ehlmann *et al.*, 2008a; Tarnas *et al.*, 2019).

Orbital spectrometers indicate the presence of carbonates throughout the region and inside the Jezero crater (Ehlmann *et al.*, 2008a). These characteristics made this paleolake a landing site of great interest for *in situ* studies and potential sample return (Ehlmann *et al.*, 2008b; McLennan *et al.*, 2011; Goudge *et al.*, 2015, 2017; Salvatore *et al.*, 2018), and they led to the selection of the Jezero crater as the landing site for the next NASA mission, Mars 2020, launched July 30, 2020. An important aspect of landing site selection for the Mars 2020 mission was the identification of deposits with high potential to preserve possible biosignatures and organic compounds that could be investigated *in situ* and cached by the Mars 2020 Perseverance rover.

The Jezero crater has been studied for more than a decade, but the timing and duration of its fluvial and lacustrine activity are still poorly constrained. Much work has focused on the western delta within the Jezero crater, with duration estimates for delta deposition and lake persistence varying from several years to millions of years, depending on studies and parameters used (Fassett and Head, 2005; Schon *et al.*, 2012; Goudge *et al.*, 2015). The fluvial valleys that fed the crater lake have also been mapped and described by previous studies (Fassett and Head, 2005; Mangold *et al.*, 2007; Goudge *et al.*, 2015), but these valleys have received much less attention than the paleolake and associated fan-delta

[1]Laboratoire Planétologie et Géodynamique, UMR6112 CNRS, Faculté des Sciences, Université de Nantes, Nantes, France.
[2]Univ Lyon, ENSL, Univ Lyon 1, CNRS, LGL-TPE, Lyon, France.
[3]Faculty of Geosciences, Utrecht University, Utrecht, The Netherlands.
[4]International Research School of Planetary Sciences, Università Gabriele D'Annunzio, Pescara, Italy.
[5]Jet Propulsion Laboratory, California Institute of Technology, Pasadena, California, USA.

deposits. Analysis of these valleys has the potential to provide new constraints on the relative timing and duration of aqueous activity in the Jezero crater, thereby helping to clarify and possibly resolve uncertainties regarding the climate during the deposition of the Jezero deposits and the persistence of conditions that are suitable for habitability at the surface. Such constraints are critical for assessing and understanding the astrobiological potential and relevance of the Jezero crater and samples collected at this site.

In this study, a geomorphologic approach is used to qualitatively and quantitatively analyze the fluvial activity that enabled the deposition of the fan-deltas inside the Jezero crater. We analyzed the morphometry of the valley networks, including transverse and longitudinal profiles, estimated discharge rates of observed channels, and analyzed their stratigraphic relationships with surrounding landforms and lithological units. These results provide new constraints on the formation of the fan-deltas in Jezero, including the age and timescale of the paleolake activity, whereas a new study focused on the delta formation will further estimate the minimum lifespan of the Jezero delta (Salese *et al.*, 2019a, 2020) by using hydrological models from the work of Kleinhans (2005, 2010). We conclude our study with a summary of the exobiological implications of our results for the Mars 2020 Perseverance rover's exploration in the Jezero crater.

2. Datasets and Methods

Data used in this study include visible images acquired for this region, including High Resolution Stereo Camera (HRSC) images (Neukum *et al.*, 2004), images from the Context Camera (CTX) (Malin *et al.*, 2007), and High Resolution Imaging Science Experiment (HiRISE) images (McEwen *et al.*, 2007). Mosaics of these images were assembled in a Geographic Information System enabling morphometric measurements and mapping. This study's morphologic assessment is placed into a broader mineralogical and lithological context by using previous studies' observations from infrared spectrometers in the Nili Fossae region (Poulet *et al.*, 2005; Mangold *et al.*, 2007; Ehlmann *et al.*, 2008b; Mustard *et al.*, 2009; Goudge *et al.*, 2015, 2017).

Regional topography was obtained from the Mars Observer Laser Altimeter (MOLA) (Smith *et al.*, 2001) and from digital elevation models (DEMs) calculated from HRSC stereo images (Gwinner *et al.*, 2010; Ansan and Mangold, 2013). For local observations of the Jezero crater entrance, DEMs were constructed by using HiRISE stereo image pairs and CTX stereo image pairs (see figure captions for image numbers). The resulting DEMs have been sampled with a spatial resolution of 1 m/pixel for HiRISE and 10 m/pixel for CTX. These DEMs were produced by stereo-photogrammetry using ''Socet set'' software (Kirk *et al.*, 2008).

Estimations of channel discharge rates Q require the knowledge of the channel width W and, depending on methods, the local slope s, channel height H, and empirical laws. Fassett and Head (2005) used the method developed by Irwin *et al.* (2005) based on the empirical knowledge of valley widths on Earth (Osterkamp and Hedman, 1982) and accounting for Mars gravity:

$$Q = 1.44W^{1.22} \quad (1)$$

A second method is based on the Manning equation initially developed for estimating discharge rates for pipelines with a correction for Mars gravity (*e.g.*, Komar, 1979; Wilson *et al.*, 2004):

$$Q = A\left(g_M \cdot s \cdot R^{4/3}/g_E n^2\right)^{1/2} \quad (2)$$

In this relation, A is the flow cross-sectional area, g_M and g_E are gravity on Mars and Earth, respectively, the local slope s is measured from topography, n is the Manning roughness coefficient, and R is the hydraulic radius, defined as the ratio of the flow cross-sectional area to the wetted perimeter. A and R are calculated by assuming a rectangular shape using the valley channel height H and width W. The friction coefficient n is fixed to 0.545, a value assumed to represent coarse-grained, clast-rich channel beds for Mars as defined in the work of Wilson *et al.* (2004). Smaller values are plausible for sandy beds, as expected for fluvial bars, but smaller values of n would increase the discharge rates.

Thus, we choose to keep the parameter at the upper bound to keep discharge rates estimated as lower bounds. A third terrestrial method uses the Darcy–Weisbach equation (Silberman *et al.*, 1963). Although less popular than Manning, this equation has been applied on several martian fluvial systems (*e.g.*, Kleinhans *et al.*, 2005, 2010; Roda *et al.*, 2014; Salese *et al.*, 2016); it is especially useful when estimations of the grain size distribution can be done and is potentially more accurate than Manning (Wilson *et al.*, 2004):

$$Q = A(8g_M Rs/f)^{1/2} \quad (3)$$

where f is a friction factor established according to the work of Kleinhans (2005) following another semi-empirical law:

$$(8/f)^{1/2} = 2.2(H/D_{50})^{-0.055} s^{-0.275} \quad (4)$$

where D_{50} is the mean grain size diameter. We will use for D_{50} the value measured in the conglomerates of Gale crater at 0.01 m (Williams *et al.*, 2013). Although this value has no reason to apply everywhere on Mars, it is the only known ground truth yet. We will provide results from the three methods to enable cross-comparisons.

3. Morphological Analysis of Fluvial Valleys Linked to Jezero Crater

3.1. Morphology and topology of valley networks

Two fluvial valleys enter into Jezero crater, Neretva Vallis to its west and an unnamed valley to the north (Fassett and Head, 2005). The basic morphology of these valleys is described first, followed by a presentation of more quantitative parameters.

3.1.1. Inlet valleys. The main tributary of Neretva Vallis extends over ~200 km west of Jezero crater (Fig. 1). This valley is linked to several secondary tributaries ranging in length from 2 to 50 km. This valley network presents a Strahler-order value of 3, indicating a network with low to moderate branching. The surrounding highlands are strongly

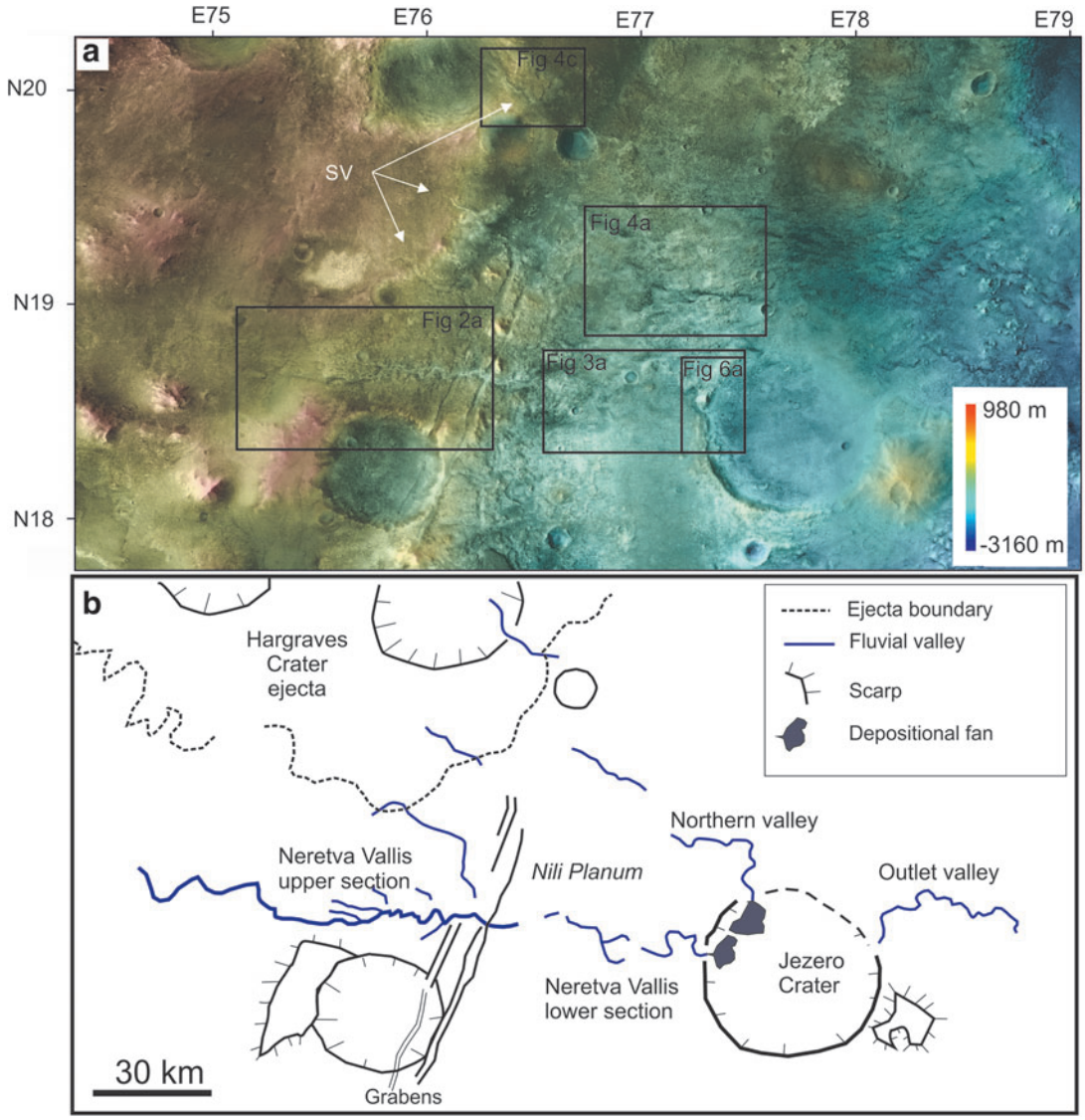

FIG. 1. **(a)** CTX mosaic merged with color topography (MOLA data) with the Jezero crater at the eastern side. SV: Small valleys without clear connection with the two main valley systems. **(b)** Simplified geomorphic map of the same area with all features of interest discussed in the study. Two fluvial valleys connect into the Jezero crater, including Neretva Vallis to the west. Hargraves crater is located further north outside the boundary of this map. Its ejecta were identified by grooved terrains. CTX, Context Camera; MOLA, Mars Observer Laser Altimeter.

etched by wind, suggesting that the smallest tributaries might have been degraded by this erosion and are not identifiable.

Over the westernmost 130 km, Neretva Vallis displays deep canyons with steep walls (maximum depth of 400 m), corresponding to substantial incision (Fig. 2). The main tributary valley is sinuous and characterized by the presence of a few bends comparable to valley meanders (Fig. 2c). Some tributaries appear to be short in length (<20 km) and display relative steep valley heads. The main tributary, however, is much more elongated and does not present an amphitheater-shaped valley head. The lack of inner channels on the floor of these valleys limits the identification of the fluvial regime. The floor is frequently covered by eolian bedforms (Fig. 2c), which limit the identification of channels in this upper section.

The easternmost 70 km of Neretva Vallis has a distinct morphology compared with the first 130 km. Its course carves into a hilly bedrock with varying widths (from 200 m to 3 km) (Fig. 3). Overall, the following observations show that the valley presents patterns that resemble more individual channels with local sedimentary deposits than a bedrock valley with a prolonged erosion from plenty of streams. First, the 70-km section of the main valley displays a flat floor and a rectangular side with apparent shallow depths (<<50 m) and a lack of branching tributaries. Second, elongated landforms of a homogeneously dark-toned material are present along the course of the valley in several locations (Figs. 3b–f), although eolian bedforms partly hide the valley floor. These elongated landforms are several hundreds to a few kms in length for a few tens of meters in width. Their location, size, and aspect are consistent with fluvial longitudinal bars.

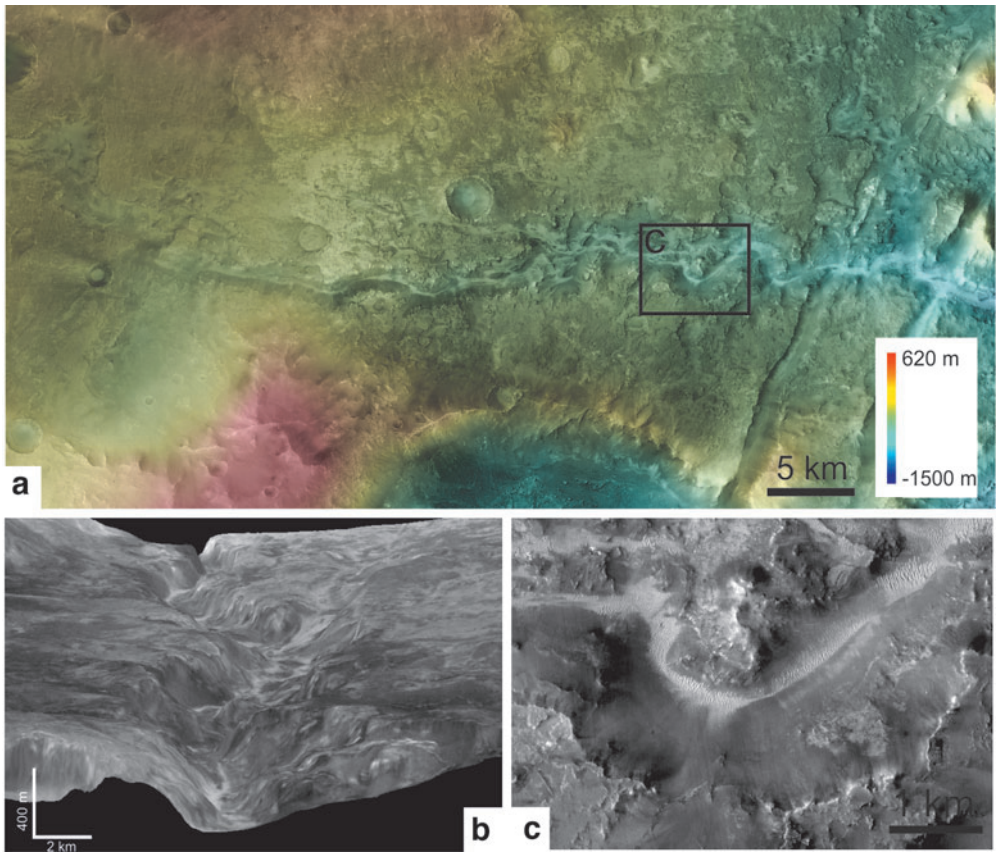

FIG. 2. **(a)** Deepest part of Neretva Vallis (CTX mosaic merged with color HRSC data DEM in transparency, orbits 988 and 1347). **(b)** Westward three-dimensional view looking upstream in the western valley network displaying a 400 m deep canyon. **(c)** CTX close-up on a sinuous part of the valley. Note the light-toned transverse dunes on valley floor. DEM, digital elevation model; HRSC, High Resolution Stereo Camera.

These landforms are not observed locally on the floor of the valley, but they are found consistently along and over its whole width (Figs. 3c–e), which means that the fluvial pattern is closer to the features classically observed for channels than to those of a fluvial valley incising bedrock. Assuming these landforms are fluvial bars, the flowing river would have been marked by successive divisions and rejoinings, as classically observed for braided rivers. This category of channel pattern can be referred to as a moderately braided type, that is, a low braiding parameter of about 1, such as defined by Rust (1978). Third, fluvial deposits have accumulated along a 3 km-wide area visible in Fig. 3c (black arrows in Fig. 3d). These deposits are partly etched by wind, but they are sufficiently preserved to enable recognition and interpretation of fluvial bars (Fig. 3e, f); whereas the valley, as a topographic depression, is no more visible in the topography, that is, the deposits have spread over this location without eroding the bedrock.

At this location, the deposits are likely the result of an amalgamation of deposits from several channels, or an accumulation of streams having spread laterally as observed for braided rivers (*e.g.*, Reading, 1996). Note that the dark material presents 10 m scale regular polygons as frequently observed in martian sedimentary deposits (*e.g.*, El Maarry *et al.*, 2012). Fourth, in one location (Fig. 3e), the fluvial patterns divide into two branches to the East and to the South. The eastern branch seems to be the first to have formed, because the E-W trending bars have been buried beneath the sediments from the N-S fluvial deposits (left of Fig. 3e). Such a change in flow direction is typically observed for channels with avulsions due to variations in discharge rates or sedimentary deposits accommodation, whereas it is uncommon for a fluvial valley to divide into two branches in the downstream direction rather than the contrary, that is, valleys branch together going downstream but do not divide (*e.g.*, Knighton, 1998). Thus, the morphology of the lower part of Neretva Vallis is dominated by patterns typical of channels without a significant erosion of the bedrock, strongly contrasting with the style of the deep valleys observed in the upper 130 km of Neretva Vallis.

The main tributary north of the Jezero crater extends over ~80 km (Fig. 1). Due to extensive surface erosion and poor incision of the valley within the substrate, this valley appears discontinuous at times, preventing a continuous trace from upstream to downstream. It is a poorly developed system showing only one minor tributary. As for the lower 70 km of Neretva Vallis, the northern valley does not show a well-defined topography (Fig. 4a). This valley develops into hilly bedrock with a rectangular shape, steep decameter-high sides, and flat floor. Although the extensive eolian bedforms on the floor complicate the interpretation, the northern valley displays elongated patterns that are also interpreted as fluvial bars, because they are similar in shape and amplitude (several 100s of meters in length) to

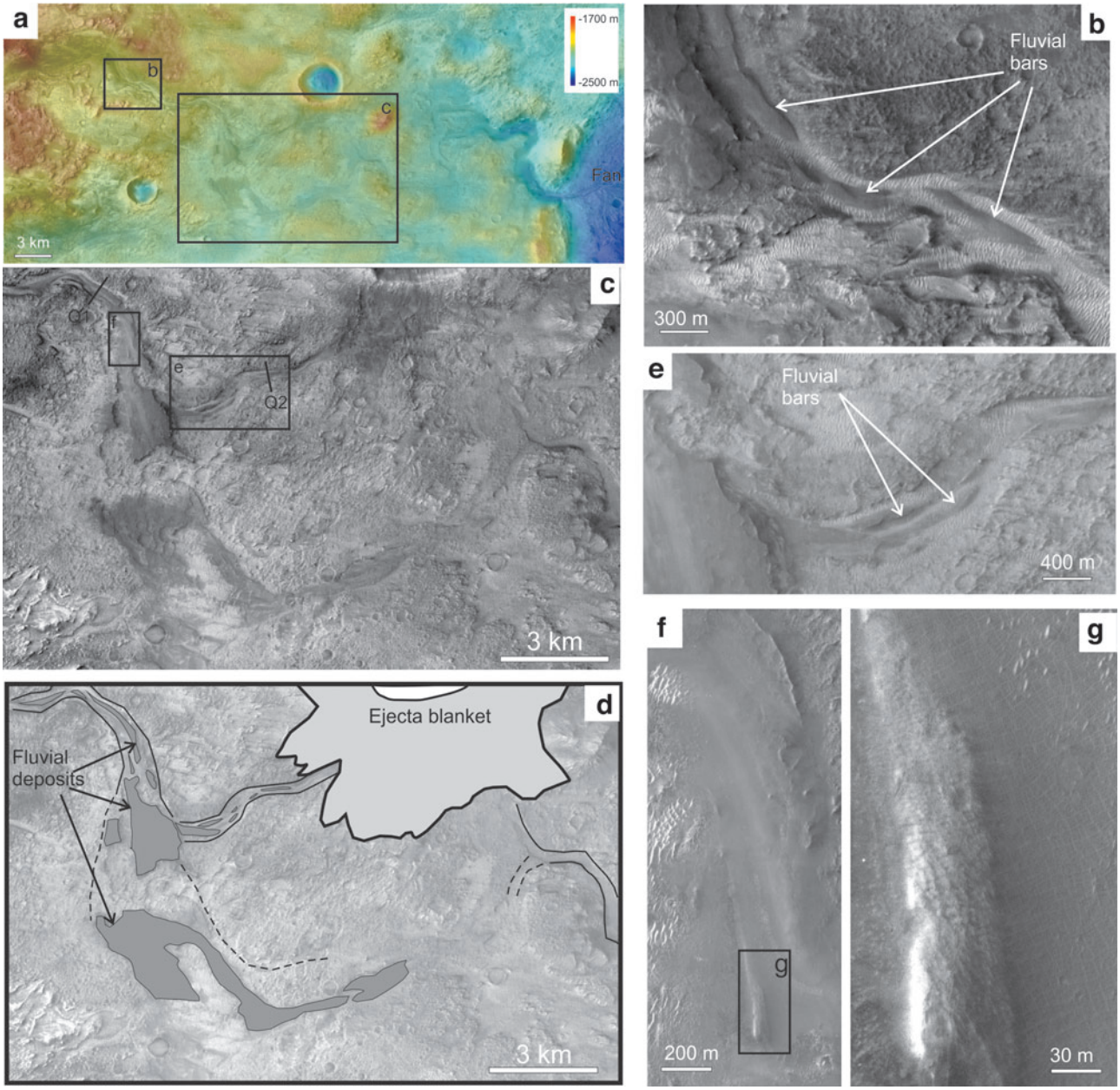

FIG. 3. **(a)** Lower section of Neretva Vallis (CTX mosaic merged with color HRSC DEM in transparency). The flow is from left to right. **(b)** Close-up showing the presence of elongated interior deposits interpreted as fluvial bars. The valley floor is blanketed by eolian bedforms. **(c, d)** Close-up on CTX **(c)** and interpretative sketch **(d)** showing a widening of the valley and a diversion into two branches to the South and to the East. Locally, the flow patterns reach 3 km in width, but they do not display any incision into the bedrock. There, dark material (gray filling pointed by black arrows in **d**) displays elongated features and is partly eroded **(f)**. Q1 and Q2 are sections at which discharge rates have been estimated (Table 2). **(e)** Close-up on the diversion to the East showing elongated features interpreted as remnants of fluvial bars. **(f, g)** Close-ups on elongated ridges interpreted as fluvial bars (HiRISE image PSP_007780_1985). The highest resolution shows that this material is covered by regularly spaced polygons of 10–20 m wide. HiRISE, High Resolution Imaging Science Experiment.

those observed in the lower section of Neretva Vallis (Fig. 4b).

Here, too, the presence of bars suggests that the valley was formed by a channel that occupied the whole width of the valley. These similarities in size, shape, and style suggest that the northern valley and the lower 70 km of the western valley formed under the same processes and potentially coevally. The faint aspect of the northern valley does not allow us to determine an accurate amount of the eroded volume or cross-sections, so we limit further quantitative developments to Neretva Vallis in sections 3.2 and 3.3.

3.1.2. Other fluvial landforms. In addition to these two main valley systems, small valleys (10 to 30 km long) are observed at the edge of Hargraves crater ejecta (Fig. 1, small valleys (SV) crossing the East of the Hargraves ejecta [Fig. 4c, d]). These valleys are oriented toward the preferential slope as are all fluvial valleys, confirming their origin,

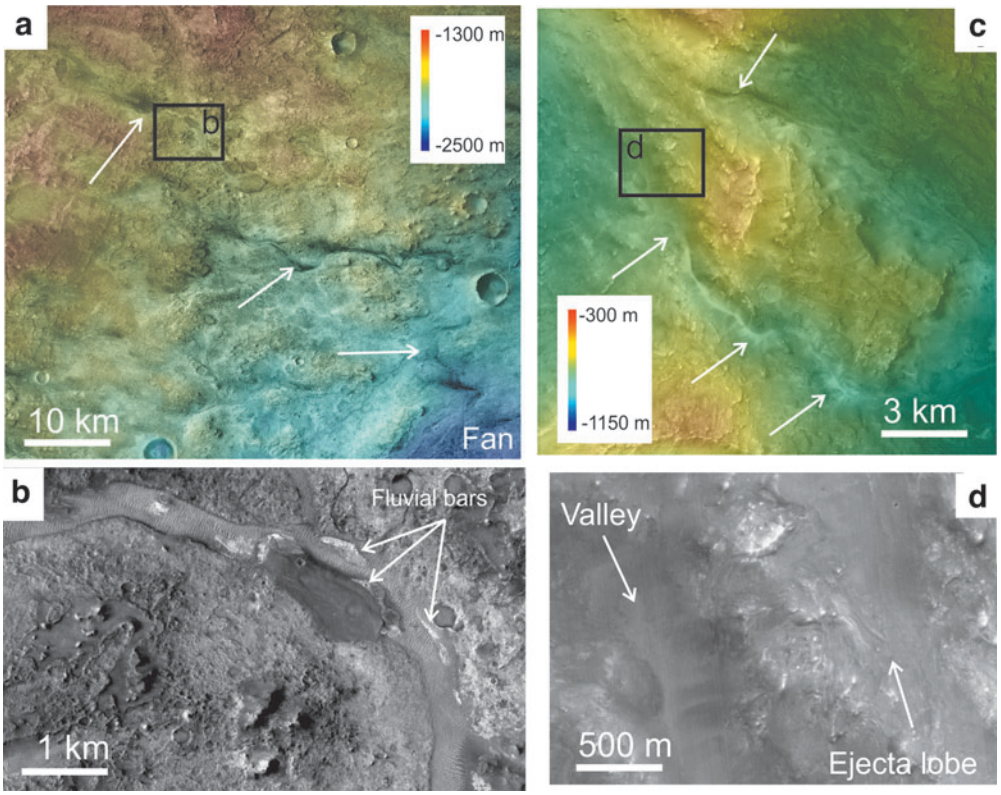

FIG. 4. **(a)** Northern valley (CTX mosaic with color HRSC DEM in transparency). Flow from upper left to bottom right. The valley is not well visible in the topography. **(b)** Close-up on CTX image of the 500 m-wide valley. The presence of fluvial bars (arrows) indicates flow features that are typical of channel deposits. **(c)** Close-up on two valley sections (white arrows) upstream of the northern valley without clear connection to the latter. **(d)** The basement is covered by Hargraves ejecta, but the valleys are blanketed by smooth eolian material discarding obvious chronological relationships.

but they lack tributaries and outlets. The valleys are located in places where ejecta from Hargraves created a rough pattern to the southwest direction. However, the valleys are filled by eolian material, and it is unclear whether or not they cut the ejecta. Thus, it is unclear whether these valleys formed before or after these ejecta. Because of their discontinuous shape, it is also unclear whether these valleys were once linked to the main valley networks and connected to the Jezero crater depositional fan-deltas.

The outlet valley east of Jezero crater displays a channel-like style over 70 km with a relief of 800 m from head to outlet. This valley decreases in width with distance to its end. The outlet valley was not investigated in this work but has been included in a numerical model and an evolutionary scenario of Jezero basin (Salese *et al.*, 2019a). This valley is generally interpreted as due to short-duration episode(s) related to the breach of the crater to the East and corresponding to short release(s) of water (<<100 years, Holo and Kite, 2017).

3.1.3. Watershed areas and drainage densities. Drainage density is a useful parameter that provides a quantitative estimation of the fluvial activity compared with other locations on Mars or Earth. The drainage density is the ratio of the total valley length over the watershed area. Fassett and Head (2005) estimated the total basin area from the sum of both northern and western watersheds to be $\sim$15,000 km^2. More recently, Goudge *et al.* (2015) estimated the catchment of the western valley as 12,000 km^2 and that of the northern valley as 18,700 km^2. These estimations have been made by a method of automatic topography extraction with the hypothesis that the Hesperian age Hargraves impact crater formed after the fluvial activity (Goudge *et al.*, 2015); the basin defined from actual topographic divide is smaller than these estimations. Because the relationships between fluvial valleys and Hargraves crater are unclear, we use manual observations of the valley heads independent of Hargraves crater to provide more conservative estimations of catchment areas. Our analyses define a smaller catchment area of 6500 km^2 for the western watershed (Neretva Vallis). The drainage density inferred for the western watershed is thus of $\sim$0.05 km^{-1}. The lack of tributaries for the northern watershed prevents constraint of the basin extension and the drainage density.

3.2. Morphometry of fluvial valleys

3.2.1. Transverse topographic profiles. Transverse topographic profiles help to quantify valley morphology (Fig. 5). The upper portion of Neretva Vallis (westernmost 130 km) is up to 4 km wide and presents deep incisions down to 400 m deep (Fig. 5b, c, sections U1 to U6). Depth and width of the main tributary increase gradually downstream (similarly to

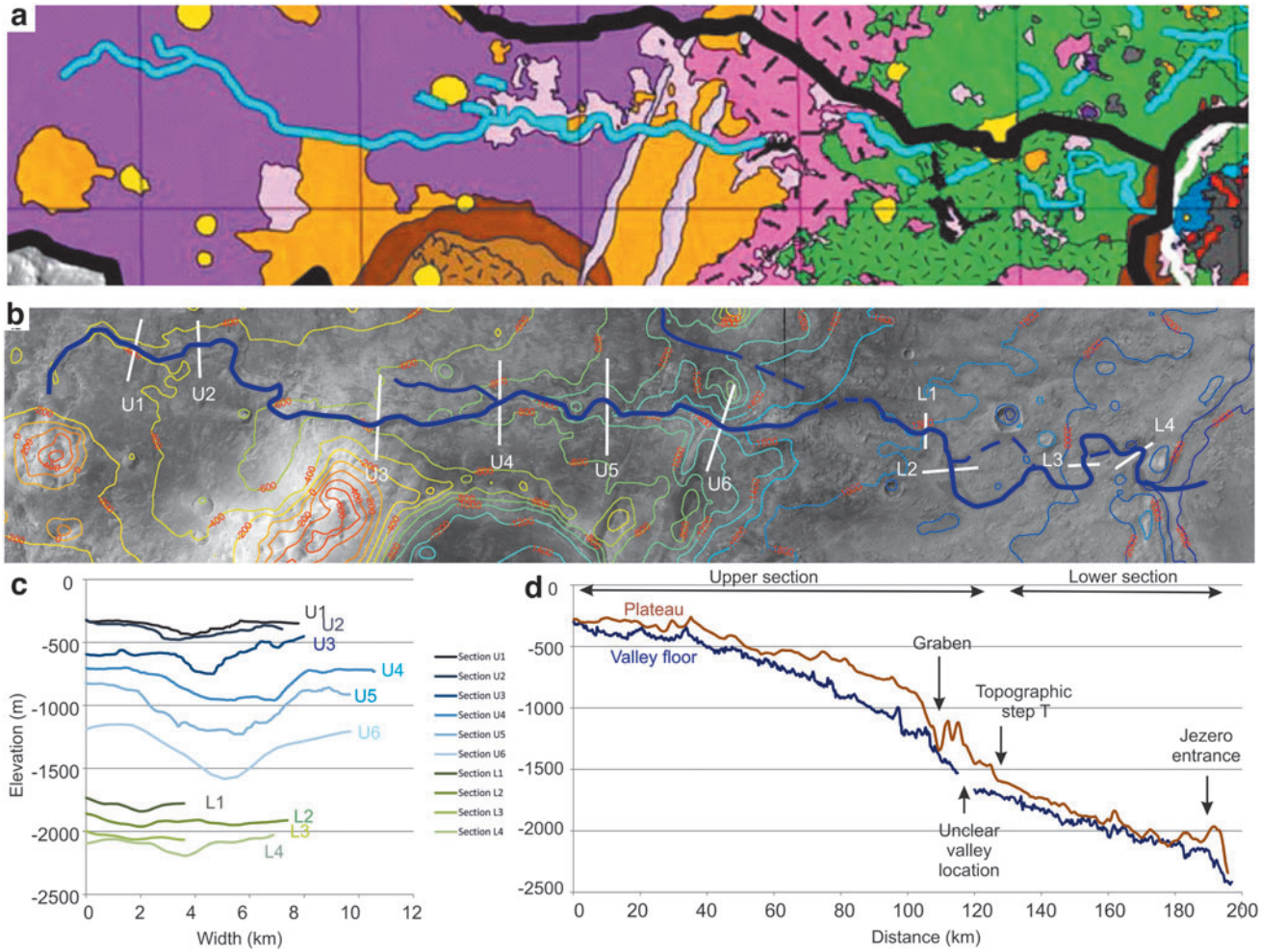

FIG. 5. **(a)** Lithology map from Goudge *et al.* (2015). Green: Mottled terrain (olivine-bearing unit). Pink: Altered basement. Purple: Pitted capping unit. Orange: Dusty, massive basement. Brown: Crater rim material. **(b)** CTX mosaic with topographic contours in color (100 m spacing), main fluvial valley in blue, and cross-section in white. **(c)** Transverse topographic profiles through the sections of valleys shown in **(b)** from U1 to U6 for the upper section and L1 to L4 for the lower section. **(d)** Longitudinal profiles of the main tributary (blue) and the surrounding plateau (brown). Note that the irregularities (local bumps) in the profiles are usually related to subsequent activities (small craters, fallen blocks, *etc.*) having modified the valley floor.

canyons carving terrestrial plateaus), which demonstrates an increase in supply related to incoming tributaries and extent in drainage area (*e.g.*, Montgomery and Gran, 2001).

In contrast, the lower 70 km-long portion of Neretva Vallis displays more subtle relief in the DEM. It shows shallow depths strictly limited to 50 m, except at the entrance of the Jezero crater where it incises the rim of the crater showing locally steep walls with a 300 m elevation difference at the rim intersection. The changes in width appear related to local variations in slope rather than a gradual increase in supply as would be the case with a number of tributaries increasing downstream. Indeed, no obvious tributary connects to Neretva Vallis in its last 70 km.

This difference in depth between the upper and lower sections of Neretva Vallis is also highlighted by the difference in eroded volume. A total eroded volume of 56 km^3 is calculated for the whole western valley system (in agreement with previous work, 58 km^3) (Fassett and Head, 2005) (Table 1). This volume takes into account only the valleys that are well defined in the topography, so it can underestimate the total eroded volume over the whole catchment. However, the upper valleys represent 95% of the volume (53 km^3), whereas the lower valley accounts for only 5% ($\sim$3 km^3) with large uncertainties ($\sim$1 km^3) that were difficult to estimate because of the lack of topographic signature in some locations. In addition, half of the volume of the lower valley ($\sim$1.5 km^3) corresponds to the last 10 km at the breach into the Jezero crater. Thus, the volume/length ratio of both portions of Neretva Vallis shows that the upper section has undergone >10 times more incisions than the lower section, with a sharp transition from one to the other east of the basement plateau (East of U6 cross-section in Fig. 5b).

3.2.2. Longitudinal profiles. Longitudinal profiles used here should be treated as first-order-magnitude estimates for the main tributary given that those profiles follow a

Table 1. Main Morphometric Parameters Measured in This Study and Compared with Previous Studies

	Previous studies	*This study*
Volume fan	5 km^3	$\sim$4 km^3
Lake level	−2395 m	$\sim$ −2400 m
Volume eroded by valleys	58 km^3	Lower valley: 3 km^3 Upper Valley: 53 km^3
Watershed area	15,000 km^2 (all) *12,000 km^2 (western watershed only)	$\sim$6500 km^2 western watershed (see section 3.1.3)
Channel width	50–100 m (on the fan)	200–500 m (upstream Jezero entrance)
Discharge rates	170–400 $m^3 \cdot s^{-1}$ (locally on the fan)	900–21,000 $m^3 \cdot s^{-1}$ (see Table 2 and section 3.3)
Strict minimum period of activity for fan formation	11 years	4 years (see section 5.1)

Previous studies from Fassett and Head (2005) and *Goudge *et al.* (2015) measured channels on the depositional fan.

topography that has been modified by more recent processes (*e.g.*, landslides, eolian activity). The longitudinal profile of Neretva Vallis displays a straight, slightly convex shape (Fig. 5d). The edge of the basement plateau triggers a change in bedrock profile, which has strong implications for the erosion. In the upper section, Neretva Vallis becomes deeper as it gets closer to the edge of the plateau, as has been observed from the transverse profiles (Fig. 5c).

The transition between the two types of valley style occurs near the location of a southwest-northeast fracture zone that also coincides with a difference in lithology between the pyroxene-bearing bedrock (west of the topographic step T) and the olivine-rich bedrock (East of T) (Fig. 5a, d). Extensive degradation of the surface complicates the identification of the main valley at this location and prevents a clear assessment of the transitions between the valleys incising the plateau and the channel-style valleys downstream.

Downstream, the channel-style valley is shallow compared with the surrounding bedrock and shows a straight longitudinal profile (Fig. 5d). The topography of the basement in this area was difficult to follow because of its hilly and irregular texture. As a consequence, the difference in elevation between the plateau and the valley in the longitudinal profile between 130 and 180 km is irregular and imprecise because the surface has been modified by degradation processes unrelated to the fluvial erosion. The difference in elevation from the point T to the Jezero crater entrance is $\sim$500 m over a straight-line distance of 50 km ($\sim$1% slope), which is steeper than that of the plateau basement (from 0% to 1%). Local slopes along the paleostreams are not significantly gentler in the lower section (0.5% to 0.8%) than in the upper section (0.5% to 1.3%). The two latter observations need to be taken into account in the understanding of the difference in style of the two parts of the valley (as discussed in section 4.1).

Lastly, at the eastern edge of the profile, there is a 200 m elevation step at the entrance of the Jezero crater, before reaching the lake deposits (−2400 m). At this location, the breach of the crater rim has created a deep valley. The difference of elevation along the valley floor is 200 m along the last 10 km (Fig. 6), including a steep topographic step of $\sim$100 m over 1 km just before the fan deposits (Fig. 6c, location X).

3.3. Fluvial regime and discharge rates

No obvious channel is observed in the upper section of Neretva Vallis, precluding any calculation of hydrological parameters in this area of the watershed. The lower section is a location where an estimate of paleo-hydrology can be performed given the presence of channel landforms. Apparent channel widths vary from 200 m to 3 km in this lower section. Alluvial deposits are locally estimated to be a few tens of meters thick, at most. We estimated the discharge rates in three locations where the valley displayed channel features suggesting that the stream occupied the whole width of the valley, at Q1 and Q2 sections (Fig. 3c) and at the entrance of the Jezero crater.

Among the three methods for discharge estimations, both Manning and Darcy-Weisbach require an estimation of the height of the channel. Using the apparent channel height is controversial and may probably due to a progressive incision in the channel rather than a single episode over its whole thickness. In addition, no HiRISE stereo images are available in key locations where the elongated landforms interpreted as fluvial bars are observed, those being too small for the HRSC DEM resolution. A 5 m-high terrace was observed at the entrance into the Jezero crater (Salese *et al.*, 2019a) that can act as a local height for the entrance channel. For the other locations, we base our estimations on empirical laws. It has been shown on Earth-based fluvial river datasets that the channel height H varies with the width W and the discharge rate Q: $H = 0.33Q^{0.35}$ and $W = 3.67Q^{0.65}$ (Hey and Thorne, 1986, Knighton, 1998, both for small terrestrial rivers). This turns out to give: $H = 0.33(W/3.67)^{0.78}$ at a given discharge rate.

These empirical results can slightly vary with Mars gravity. According to Irwin *et al.* (2005), depending on the channel type, the height:width ratio can be down to 0.7 times the value it has on Earth because of the gravity difference. To provide conservative values, we use these lowest bounds to provide a channel height that is not overestimated in the three locations considered (rounded to the closest integer, results give 5 m at 200 m width and 10 m at 500 m width). These values are consistent with recent scaling relationships introduced by Konsoer *et al.* (2018) and with the value measured from a terrace at the channel entrance into the Jezero crater by Salese *et al.* (2019a), estimated to be 5 m depth for a width of 190 m.

Discharge rates estimated at three locations along the lower section of the valley and at the entrance channel vary from 900 to 21,000 $m^3 \cdot s^{-1}$ by combining the extreme values of the three methods (Table 2). The comparison between the three methods gives a sense of the potentially large uncertainties related to these calculations. However, despite these large uncertainties, all methods point toward relatively high discharge rates (10^3 to 10^4 $m^3 \cdot s^{-1}$) in the three locations where these calculations have been made. These

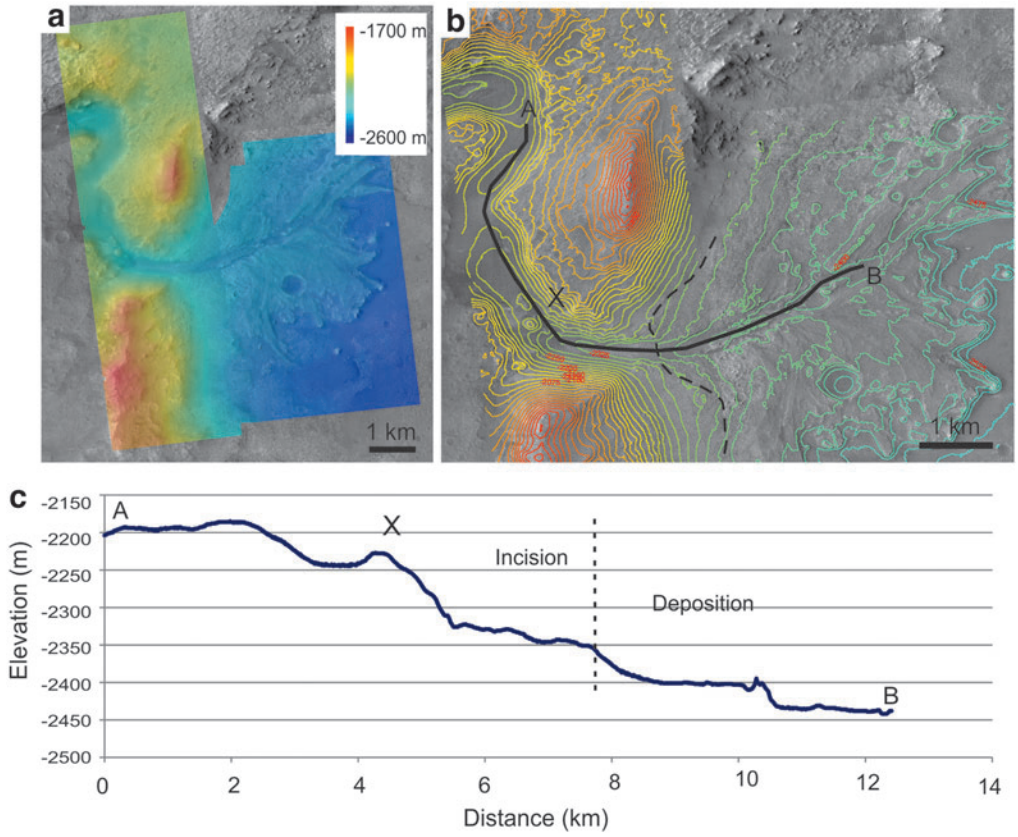

FIG. 6. **(a)** Mosaic of CTX and HiRISE images with merged HiRISE DEMs in color (from west to east: ESP_036618_1985 and ESP_037119_1985, ESP_042315_1985 and ESP_037396_1985, PSP_002387_1985 and PSP_003798_1985) at the entrance of the Jezero crater. **(b)** Close-up of the entrance of the Jezero crater. The topography of the 12 km-long transversal profile A–B is detailed in **(c)**. The difference of elevation is of 200 m from A to the start of the depositional fan. The location X is a knickpoint with a steep slope of 10% (100 m of elevation in 1 km) preceded by a local low linked to scouring before a resistant obstacle.

estimations of discharge rates are only valid for the last episodes of flow, possibly linked to the entrenchment of the depositional fan at its entrance (Fig. 6).

3.4. Interpretations of geomorphological results

3.4.1. Interpretation of the longitudinal profiles. Longitudinal valley profiles enable estimation of the degree of equilibrium of valleys, linked to their process of formation and potentially their duration of activity (*e.g.*, Knighton, 1998; Charlton, 2007). Concave profiles are expected for river at equilibrium, although recent progress on terrestrial works shows that landscape evolution may not always lead to an ultimately concave profile (*e.g.*, Willett *et al.*, 2018). Indeed, the longitudinal profile of a river profile depends on (1) the variations in discharge rate along the river and, therefore, the number of incoming tributaries, (2) the base level (sea level on Earth, the Jezero crater floor and lake), (3) the pre-existing topography and/or tectonic context, and (4) the climatic conditions. For instance, on Earth, arid-zone streams have limited concavity or convex shapes due to the lack of tributaries downstream as well as the loss of water by evaporation and infiltration (Knighton, 1998; Willett *et al.*, 2018). The topography used here is a first-order estimation

Table 2. Channel Discharge Rates at Four Locations Along the Lower Valley at Locations Q1 and Q2 (in Fig. 3c) and at the Entrance Channel in Fig. 6c (Location of the Dotted Line)

			Discharge rates ($m^3 \cdot s^{-1}$)		
Location	*Width (m)*	*Slope*	*Empirical*	*Manning*	*Darcy-Weisbach*
Q1 (Fig. 3c)	500	0.007	2826	21,303	9954
Q2 (Fig. 3c)	200	0.017	924	4161	1778
Q3 (entrance channel)	200	0.014	924	3776	1702

Three methods were used: The empirical width/depth ratio (Irwin *et al.*, 2005), the Manning equation (Wilson *et al.*, 2004), and the Darcy–Weisbach equation (Kleinhans *et al.*, 2010).

of the profile, because a precise profile cannot follow the exact location of the past river (no channel visible in the upper part), and craters or landslides could have modified the shape locally. Keeping in mind these limitations, longitudinal profiles can inform us on the evolution of the valley system.

None of the investigated sections of the longitudinal profile for Neretva Vallis is concave. Profiles are either slightly convex or straight (Fig. 5d). The slightly convex profile of the upper valley section can be explained by the presence of the topographic step at the edge of the plateau, which is progressively dissected (Fig. 7a). This part of the longitudinal profile is linked to progressive backward erosion, which is related either to normal faults present at the eastern edge of the plateau that lowered down the base level progressively, or to the resistant lithology of the plateau, or both. An equilibrium (concave profile) was not reached likely because of the low number of tributaries and the substantial thickness (400 m) of plateau to erode.

This poorly dendritic network of deep valleys has some similarities in shape with valley networks such as Nanedi or Nirgal Valles, with tributaries showing amphitheater heads and steep valley walls. Steep valley heads with amphitheaters have been interpreted as sapping valleys in the past (*e.g.*, Pieri, 1980; Laity and Malin, 1985; Malin and Carr, 1999), that is, formed by deep subsurface flow, groundwater seepage, and related erosion. Those valleys have been taken in the past as an indicator of flows limited to the subsurface (*e.g.*, Goldspiel and Squyres, 2000), but it has been shown that recharges of aquifers from the surface are needed for such processes to occur and that overland flows are required both on Earth and on Mars (Howard, 1986; Craddock and Howard, 2002; Irwin *et al.*, 2008; Lamb *et al.*, 2008; Mangold *et al.*, 2008; Lapotre and Lamb, 2018). Volcanic bedrock, especially basalts, has moderate porosity (10–30%) but includes some of the most permeable formations on Earth (Davis and De Wiest, 1966; MacDonald *et al.*, 1983; Gulick, 1998).

According to Goudge *et al.* (2015), these valleys are carved within a basaltic capping unit, suggesting that groundwater may have been involved in combination with overland flows, as observed elsewhere on Mars (*e.g.*, Salese *et al.*, 2019b). However, although the valleys present a paucity of downstream tributaries, their longitudinal and transverse profiles show that the main tributary has neither amphitheater head nor constant valley width as usually observed for sapping, but rather a progressive incision into the plateau with gradual deepening and enlargement of the main tributary (Fig. 5c) as observed for erosion dominated by overland flow. Lastly, the sinuous shape of the valley in the plateau is created by progressive incisions inherited from an initial state, possibly involving alluvial meandering channels (Johnson, 2016). Progressive incision by overland

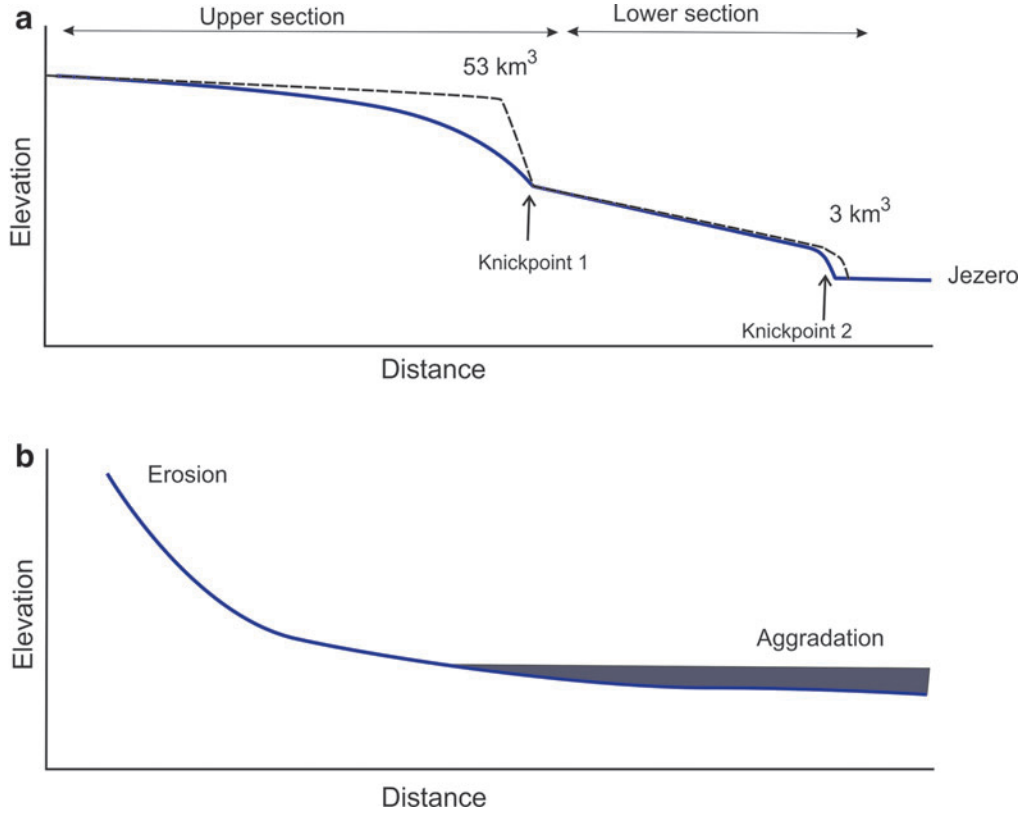

FIG. 7. **(a)** Simplified sketch of the longitudinal profile of Neretva Vallis with the upper section incising into the basement and the lower section incising poorly into the olivine-rich unit and the Jezero crater rim. The convex profile of the upper section is similar to a knickpoint controlled by normal faults and/or resistant lithology of the basement. The entrance into the Jezero crater of the lower section corresponds to a knickpoint formed by the change in base level after the flow cut into the crater rims. **(b)** Ideal longitudinal profile of a long-term river with alluvial deposition at low gradient downstream (adapted from Charlton, 2007).

flows of an igneous basement certainly requires geologically long periods (>10,000 years), although estimations of durations are difficult and generally reported to be >100,000 for Mars valley networks (*e.g.*, Gulick and Baker, 1990; Carr and Chuang, 1997; Gulick, 2001; Howard *et al.*, 2005).

In contrast, the very straight longitudinal profile of the lower section can be explained by the lack of tributaries; there is no downstream increase in stream power, and thus, there is similar erosional strength throughout the length of the valley without downward increase. Coupled with the low eroded volume and the presence of channel features, this straight profile is indicative of an immature valley, therefore distinct from the upper Neretva Vallis.

The drop in elevation at the Jezero crater entrance (Fig. 6) represents a change in base level that is interpreted as a knickpoint that did not propagate much backward, in agreement with the immature morphology of the lower valley section. Note that this drop in elevation does not correspond to the location where the river entered into the paleolake (−2395 m of elevation, Fassett and Head, 2005) and where sedimentary deposits start to accumulate. Between A and X (Fig. 6c), the longitudinal profile exhibits two small depressions that may be related to perched pools and/or local scouring of the bedrock, suggesting that the flow at this location was energetic (*i.e.*, as rapids), as expected for such a drop in topography on a short distance. Such a step is typical of knickpoints due to backward incision related to a change in the base level (*e.g.*, Berlin and Anderson, 2009; Valla *et al.*, 2010; Forster and Kelsey, 2012), here linked to the breach of the Jezero crater rim.

3.4.2. Interpretation of the differences in morphology. Morphological results highlight a strong difference in fluvial style between the channel-free, upper 130 km of Neretva Vallis that incises strongly into the basement and the tributary-free, channel-like morphology observed in the lower 70 km of Neretva Vallis and along the whole length of the northern valley. Two interpretations are possible at this stage: (A) The two styles formed coevally and the difference in morphology is related to the change in flow parameters (slopes, discharge rates, *etc.*) along the valley, or (B) the two regimes were not coeval, that is, the western valley formed in two (or more) distinct episodes.

The longitudinal profile in Fig. 5d is composed of two parts (as schematized on Fig. 7a), with a lower straight section dominated by braided streams and alluvial deposits, characteristic of aggradation, distinct from the upstream section dominated by erosion. Such a profile is observed on Earth in the case of alluvial systems. For such a scenario (A) to be valid, the lower, aggradation section should correspond to flatter areas with significant sedimentary accumulation (alluvial plains) and should not display direct incision into the bedrock as observed upstream. However, local slopes along valleys in the western basin are not significantly gentler in the lower section (0.5% to 0.8%) than in the upper section (0.5% to 1.3%). In addition, the lower section of Neretva Vallis incises into the olivine-rich bedrock (Fig. 5b) without obvious alluvial deposits apart from the elongated deposits present inside the valley (Fig. 3d), contrary to scenario (A).

Another question linked to alluvial deposition is related to where the eroded volume of the upper valleys (53 km^3) has been deposited. It has been shown that many deltaic deposits on Mars follow a volume ratio of erosion to delta that is close to one, therefore suggesting single episodes and limited dispersion of sediments within the corresponding basins (Vaz *et al.*, 2018). Thus, the volume eroded should fit the volume of deposited sediments in alluvial deposits and the fan-delta. The dark-toned deposits interpreted as fluvial bars and alluvial deposits in the lower valley represent $<<1$ km^3 of volume, far from the order of magnitude of the basement erosion and are thus not a significant sink. The observed depositional fan deposits within the Jezero crater occupy a volume of $\sim$4–5 km^3 depending on estimations (Fassett and Head, 2005) (Table 1). This is much less than the total eroded volume as well. The eroded surface of the fan and residual buttes located in front of the fan may sign a former extension before its erosion by wind (Goudge *et al.*, 2018).

The volume of the eroded part of the fan has been estimated to $\sim$2.7 km^3 in addition to its current volume (Goudge *et al.*, 2018), thus totaling 7–8 km^3 for its initial volume. This volume is still much insufficient to fill the gap of volume with that recorded by erosion, making Jezero crater an anomaly in the results reported by Vaz *et al.* (2018). Note that a change in volume from the erosional part to the deposition fan is possibly based on terrestrial observations, but it is usually considered to increase the volume of deposits because the porosity of crustal rocks is lower than that of delta sediments before compaction (*e.g.*, Reading, 1996), as would be the case of the poorly buried Jezero crater fans.

Further evidence against interpretation (A) comes from the presence of two knickpoints in the longitudinal profile. On one hand, the slightly convex topography upstream grabens can be compared with a knickpoint (knickpoint 1 in Fig. 7) due to the backward propagation of the edge of the plateau progressively incised by fluvial erosion. On the other hand, the entrance in Jezero crater is characterized by a steep slope over $\sim$1 km (Fig. 5d, knickpoint 2 on Fig. 7a). Bedrock rivers have knickpoint migration rates ranging from 0.001 to 30 m/y, with a strong dependence on drainage areas (Loget and Vand Den Driessche, 2009). In the Alps, knickpoints initiated at the same period in the same region have the same order of magnitude in backward incision (Valla *et al.*, 2010). Valla *et al.* (2010) found that knickpoint retreat rates vary with drainage area first, whereas change in bedrock lithology is a secondary parameter. Thus, along a given river, knickpoints should display a higher step downstream (larger basin) than upstream (smaller basin), as the drainage area increases downstream. At least, it should be of the same order of magnitude downstream as upstream assuming constant supply due to lack of incoming tributaries in the lowermost part of the basin.

However, the backward incision of the upper section is of ca. 80 km into the basement, whereas the backward incision observed at the Jezero entrance is of only $\sim$1 km. In addition, the difference in estimated eroded volume is large (53 vs. 3 km^3). The huge difference makes it unlikely that the same volume of water that transited into the upper section forming this strong incision would have transited through the observed breach of the Jezero crater, or the knickpoint at this location would have migrated back much further. Thus, the comparison between the two knickpoints is consistent with a difference in fluvial regimes, with a longer duration of activity in the upper valley, as suggested by the longitudinal profiles.

These observations confirm the inconsistency in morphometry between the upper Neretva Vallis and the lower poorly developed channels, suggesting a distinct evolution as in interpretation (B). In this context, it may not be a coincidence that the difference in style between the strong valley incision to the west and the limited channel incision to the east starts at the transition between two lithologies (Fig. 5). Indeed, the upper Neretva Vallis activity may have been active earlier than the lower valley section, implying that the fluvial bars and channel-type features observed downstream are not genetically linked to the same fluvial erosion that carved the canyons observed in the upstream section. Such an interpretation requires evaluating whether or not the change of lithology invoked could actually be responsible for a change in erosion style.

Rock strength is an important parameter that influences landscape erosion and fluvial incision (*e.g.*, Bursztyn *et al.*, 2015). The question raised is whether the change in lithology from the crustal basement and plateau cap rocks into the olivine-bearing unit (Fig. 5a) could constitute an explanation for the difference in morphology between the upstream and downstream parts of the valley. Assuming that rock strength is the key parameter, the difference in eroded volume downstream would imply a higher strength of the olivine-bearing unit compared with the rocks of the basement.

However, new studies interpret the olivine-bearing unit to be cemented ash deposits, especially based on the texture of this unit, which appears to be weak, and based on the fact that it does not retain well small-impact craters to erosion (Mandon *et al.*, 2020). The moderate thermal inertia, the presence of yardangs and of a sparse regolith cover also indicate that the olivine-bearing unit is composed predominantly of friable clastic rocks (Bramble *et al.*, 2017; Rogers *et al.*, 2018; Kremer *et al.*, 2019). So, this unit should be easier to erode by fluvial processes than the resistant basement upstream, contrary to what is deduced from the morphological analysis, thus confirming and enhancing the inconsistency between the two sections of the valley.

Lastly, interpretation (B) requires evaluating the relative ages of the landforms and bedrock units, given that, in such a scenario, the olivine-bearing unit should be younger than the cap rock basement and older than the fan-delta. The next section will develop these questions on the age of the fluvial activity before proposing a complete scenario.

4. Age of the Fluvial System

4.1. Chronological relationships with surrounding landforms and geological units

The plateau in the western part of the basin provided the topography for the formation of the upper Neretva Vallis; this Noachian plateau, therefore, predates the fluvial valleys. Neretva Vallis displays a change in style at the change in lithology at Nili Planum (Fig. 1), between the Noachian basement and the olivine-rich unit (Fig. 5). The olivine-rich unit clearly postdates the Noachian basement (Hoefen *et al.*, 2003; Hamilton and Christensen, 2005; Mustard *et al.*, 2008) and appears to drape the pre-existing topography in a region roughly bounded by Nili Fossae to the west and Isidis basin to the east (Ehlmann and Mustard, 2012; Bramble *et al.*, 2017; Kremer *et al.*, 2019; Mandon *et al.*, 2020). Its age remains unclear, although Middle to Late Noachian is the most likely (Mandon *et al.*, 2020.). Fluvial valleys cut the olivine-rich unit, but only those valleys that are poorly developed, braided, and channel like such as the lower section of the western valley and the northern valley. Inside the Jezero crater, the fan-deltas can be compared with surrounding units. The delta sits on the olivine-rich unit, confirming a previous observation, whereas the floor unit appears to postdate the fan-delta (Goudge *et al.*, 2015). The impact craters superposed on this floor unit give a model age of 2.6 ± 0.5 Ga in the Hartmann system, placing it in the Early Amazonian (Shahrzad *et al.*, 2019), thus providing an upper bound for the age of the delta deposition.

Crosscutting relationships with impact craters can also provide useful information. The Jezero crater is interpreted to be Noachian in age (Ehlmann *et al.*, 2009; Goudge *et al.*, 2015), in accordance with its degraded morphology and the lack of obvious ejecta typical of craters of that period (Mangold *et al.*, 2012a). However, the crater itself provides little information about the age of the fluvial activity. In contrast, the ejecta of the Hargraves crater (northwest of the area of interest, Fig. 1) drapes part of the Early Hesperian lavas of Syrtis Major Planum in Nili Fossae (Mangold *et al.*, 2007; Mustard *et al.*, 2009), providing an Early Hesperian maximum age for the crater formation. Thus, the Hargraves ejecta blanket represents an important stratigraphic marker.

According to Goudge *et al.* (2015), the Jezero inlet valleys are Noachian and predate Hargraves crater formation. However, there is no indication that any valleys are buried by Hargraves ejecta, neither for the western nor for the northern system. In contrast, small fluvial valleys cut its ejecta (SV in Fig. 1). The relationship between the ejecta and the main valley systems remains unclear, due to the strong etching of the bedrock, and it is not possible to conclude definitively whether those small valleys are coeval to Neretva Vallis or not. Nevertheless, small fluvial valleys observed inside Hargraves ejecta point toward the occurrence of some post-Noachian fluvial activity that postdated the Hargraves impact.

Considering relationships with tectonic features, the valleys postdate the SW-NE system of grabens that cut into the Noachian basement, but not into Syrtis Major Hesperian plains. Nevertheless, those grabens are deep (down to 300 m) and have not deflected the valleys toward SW or NE directions, or any deflection is no longer visible (Fig. 1). A coeval evolution of grabens and valleys is also possible.

4.2. Age of the fluvial activity from crater counts

Crater-count techniques are commonly used for dating surface of a given age, such as well-defined volcanic plains (*e.g.*, Hartmann and Neukum, 2001). Dating linear features such as fluvial valleys cannot be performed in exactly the same way. Buffered crater counts are most commonly used to date linear features, because they take into account the fact that the surface area over which the count should be performed is a function of crater diameter (*e.g.*, Tanaka, 1982).

Fassett and Head (2008) have used this technique by considering the area around the valley segments inside valley networks, assuming that all valleys of a given network are coeval. For the basin upstream of the Jezero crater, they found a Late Noachian age (3.74 ± 0.14 Gy following the Hartmann chronology). However, this technique is

powerful for dense, widespread valley networks, but statistically limited for networks with a few tributaries. Only seven craters of more than 2 km were counted for Jezero basin, including Hargraves crater. However, Hargraves crater is Hesperian with unclear relationships with the inlet valleys entering into the Jezero crater, so it should not be included in such a count. In addition, its large diameter (60 km) makes a strong load on the estimation, questioning the validity of the age found. Given the limited basin area and valley number, we choose not to reproduce such a buffered count.

To still provide a crater count age for the fluvial activity, we chose to perform a crater count of the western fan-delta. Several craters are observed on the top of the main remnant fan-deltas of the Jezero crater or affecting its edge (Fig. 8). The size frequency distribution of the craters shows that craters larger than 250 m follow isochrons quite well, whereas the distribution of the craters smaller than 250 m does not follow any of the isochrons. To estimate the age of the surface, we can use 10 craters larger than 250 m, which postdates the fan-delta (Fig. 8). Despite the low statistical sampling, these 10 craters align along the 3.5 Gy isochron, with some error bars related to the low statistical sampling giving possible ages from 3.2 to 3.6 Gy, thus leading to a Hesperian age.

The 3.2 Gy lower bound can be used as a minimum age in agreement with the crater counts that were done on the postdating floor unit that returns an age of 2.6 ± 0.5 Gy (Shahrzad *et al.*, 2019). The craters lower than 250 m with a distribution lower than the isochrons imply continuous crater obliteration/degradation (*e.g.*, Quantin-Nataf *et al.*, 2019). This is consistent with the partly eroded texture of the fan-delta surface, likely connected to the eolian erosion over >3 Gy. Although only the craters smaller than 250 m have been clearly affected by this degradation, we cannot rule out that some erosion may have affected the cratering record of craters larger than 250 m as well, leading to an underestimation of the model age, thus opening the possibility to slightly older ages than the 3.6 Gy upper bound provided by the crater count.

In summary, from crosscutting relationships, the formation of the fan-deltas, thus of the last phase of the Jezero fluvial activity, postdates the formation of the olivine-rich unit (MN-LN) and predates the formation of the floor unit (EA). From crater counts, an Early or Late Hesperian age ($3.5 + 0.1/-0.3$ Gy) is favored, ruling Amazonian ages, but a Late Noachian age is still possible assuming missing craters related to a surface degradation of the fan-delta. Thus, from crater counts and crosscutting relationships, we cannot conclude definitively about the age of the fan-delta formation, leaving open a Late Noachian or Hesperian age of formation.

5. Discussion

5.1. Scenario and period of formation of fluvial landforms

Neretva Vallis is divided into an upper section (130 km long) with significant fluvial activity inferred from the presence of deep canyons cutting into the basement plateau, and a lower section (70 km long) with much lower eroded volume and immature valley development. Quantitative parameters do not plead in favor of a common evolution of the two fluvial styles. Formation of the olivine-rich unit between the two episodes of valley formation would explain why the level of erosion observed upstream is not observed on the downstream section. We present a scenario that takes into account these observations and interpretations (Fig. 9):

(1) The basement is subjected to relatively intense erosion (53 km^3 at minimum) from precipitation (rainfall

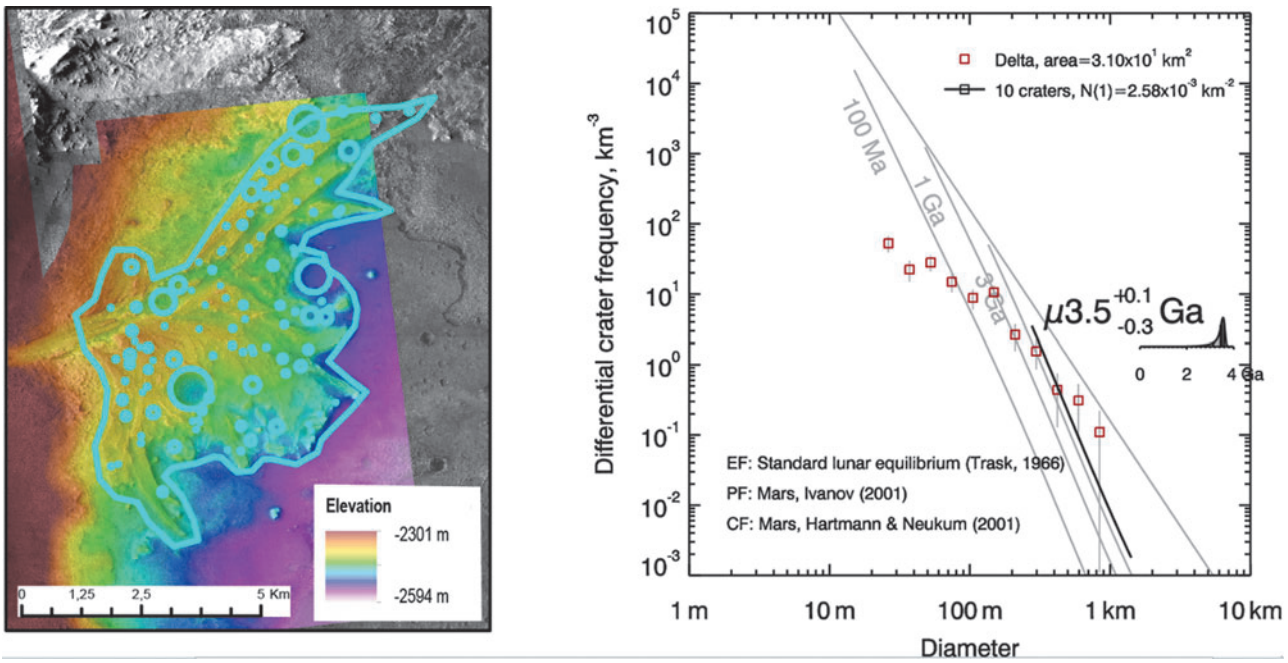

FIG. 8. Left: CTX DEM (J03_045994_1986 and J03_046060_1986_XN_18N282W) over HiRISE image mosaic on top of which the counted area and the mapped craters are highlighted in light blue. Right: Crater size frequency distribution obtained from the craterstat software (Michael and Neukum, 2010). The age is the best fit for the 10 craters that are larger than 250 m. CF, crater frequency; EF, equilibrium function; PF, production function.

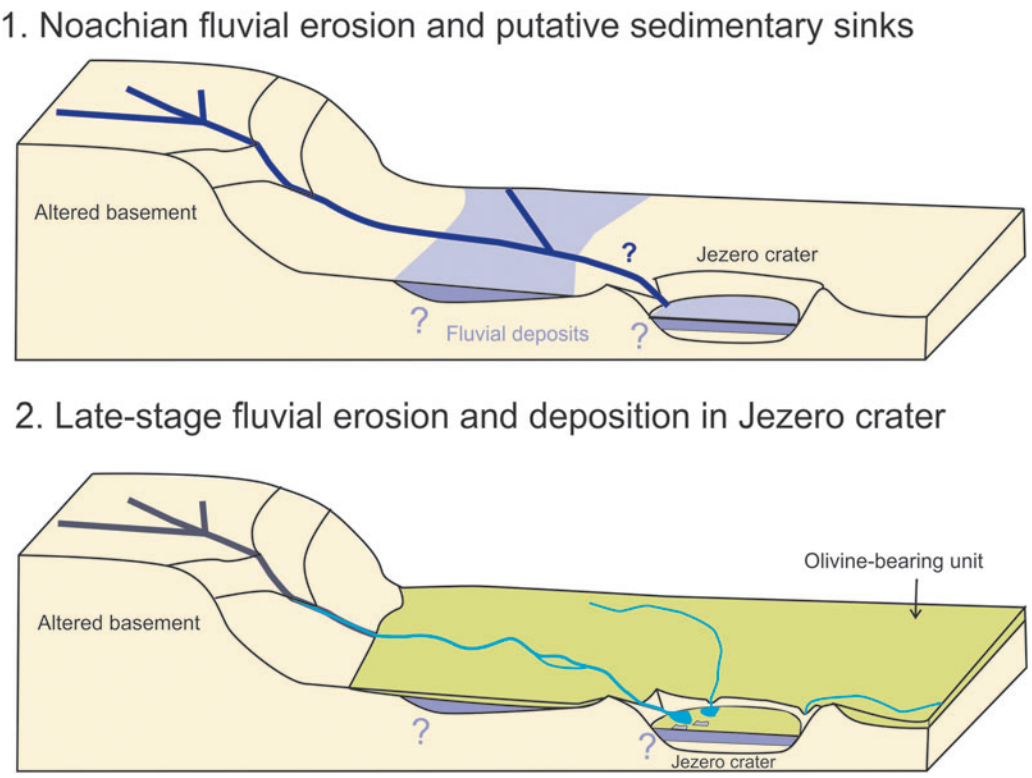

FIG. 9. Scenario of the two-stage formation of the Jezero crater fluvial activity. **(a)** Prolonged erosion of the basement during the Noachian period. Deposits from this period would have accumulated inside foothills or inside the Jezero crater through an initial breach into rims. **(b)** Reactivation of the fluvial system after the formation of the olivine-rich unit with formation of the depositional fans.

and/or snow deposition and melting) with development of deep valley networks (>100 m deep). Sediments eroded by this fluvial activity were deposited downward in two possible locations, either in topographic lows west of Jezero or inside the Jezero crater, which is a regional low area and was already present at that period.

(2) The olivine-rich unit blanketed the eastern part of the valley network, as well as sediment deposits during the first phase of fluvial activity, and the interior and rim of the Jezero crater, at least partly, burying any former fluvial and lacustrine deposits deposited in this area.

(3) The valley system was reactivated, either in continuity of the previous phase or, independently and later, forming the lower western valley (Neretva Vallis) and the northern valley at the same time. The observed fan-deltas formed as a result of this second stage of activity.

According to this scenario, the fluvial activity carving the upper valley would have started before the olivine-rich unit was emplaced, thus likely during the Middle Noachian. Morphologically, the upper Neretva Vallis fits the valleys formed in the Middle to Late Noachian on volcanic plateaus (*e.g.*, Fassett and Head, 2008). It displays a drainage density of ~ 0.05 km^{-1}, which is common in martian highlands (Carr and Chuang, 1997). The Strahler order of 3 is relatively low, compared with 4 or 5 in densely incised martian highlands (Ansan and Mangold, 2013), but reasons for the low degree of branching of valleys and moderate density can be related to various parameters such as permeable bedrock, precipitation concentrated on one region of the basin or local groundwater seepage, or a combination (*e.g.*, Knighton, 1998). In the absence of inner channels, a reconstitution of the paleohydrology and the duration of erosion is not possible. Based on Earth and Mars studies, the minimum duration of well-developed valley networks formation is usually considered to be in the range of 0.1 to 10 My (*e.g.*, Carr and Chuang, 1997; Gulick, 2001; Howard *et al.*, 2005).

In contrast, the ages of the lower valley section of Neretva Vallis and of the northern valley remain unconstrained, Late Noachian or Hesperian. These uncertainties require looking at other fluvial landforms in this region and on the whole planet for a better understanding of their period of formation. The pristine fluvial landforms of the lower and northern valleys do not share similarities with Noachian valleys observed elsewhere on Mars. Channels in well-developed fluvial Noachian valleys on Mars are locally visible on the floor of valleys (*e.g.*, Irwin *et al.*, 2005), but they are substantially narrower and shallower (>10 times) than the valleys in which they are observed, as expected for fluvial erosion.

The fluvial landforms are relatively fresh-looking, and they have similarities with small outflow channels (*e.g.*, Carr, 1987; Baker *et al.*, 1992) or late-stage fluvial landforms. For instance, fluvial bars and braided streams are observed in the Late Hesperian outflow channel Okavango

Valles (Mangold and Howard, 2013) or in Amazonian braided streams (Adeli *et al.*, 2016). Apparent local discontinuity in flows also exist on valleys of the NE rim of the Hellas basin where a series of small valleys named Navua Valles (Hargitai *et al.*, 2017, 2018, 2019) resemble in geometry (local braiding and avulsions, poor branching) and size (tens of km long) the lower western valley and the northern valley at the Jezero crater. Navua Valles channel and valley systems have been interpreted as due to periodic fluvial episodes resulting from localized orographic highland precipitation and from snowmelt or hydrothermal groundwater outflow from volcanic and impact crater sources extending from the Noachian to the Amazonian (Hargitai *et al.*, 2017, 2018, 2019).

Reactivation of Noachian valleys is not a new observation, as has been observed in Viking images (Baker and Partridge, 1986). Hesperian or Amazonian fluvial episodes on Mars have been observed in several locations and display valleys similar to channels, as suggested here for the lower sections. Although lower in intensity than the Late Noachian fluvial stage, these late-stage episodes represent significant fluvial erosion (*e.g.*, Kite *et al.*, 2019).

Many depositional fans of the same range of size as the Jezero crater are known to be Hesperian in age, for instance at Eberswalde crater (Mangold *et al.*, 2012b), in Valles Marineris area (Quantin *et al.*, 2005; Di Achille *et al.*, 2007) or in Xanthe Terra (Hauber *et al.*, 2009). Regionally, the presence of an alluvial fan inside the Hesperian crater Hargraves (Mangold *et al.*, 2007; Goudge *et al.*, 2015), small valleys cutting the Hargraves ejecta (Fig. 1), and braided channels in the surrounding of the Hesperian Syrtis Major lava flows (Mangold *et al.*, 2008) show that the fluvial activity in this region extended well into the Hesperian period.

The origin of late-stage fluvial activity remains debated: Climatic episodes including snowmelt and glacial melting perhaps related to obliquity variations (*e.g.*, Kite *et al.*, 2017), punctual volcanic activity (*e.g.*, Gulick and Baker, 1990; Gulick, 1998, 2001; Hauber *et al.*, 2005), or impact craters (*e.g.*, Segura *et al.*, 2008; Jones *et al.*, 2011; Mangold, 2012) can generate episodic activities. The crater Hargraves is large enough to have generated melting of any subsurface ice, and Syrtis Major volcanism could have created a regional source of heat for melting of ice (Hiesinger and Head, 2004). However, there is no direct evidence for the role of glacial ice, permafrost melting, or snowmelt in the upstream regions. So, a late-stage aqueous episode forming the depositional fans at the Jezero crater would remain of unclear origin.

Lastly, data from channel widths and discharge rates can be used to estimate the minimum duration of the fluvial activity related to the last phase of activity. As an example, from the fan volume, we can estimate a minimum duration taken to transport the $\sim$4–5 km^3 of sediments of the fan, assuming continuous filling and a given water:rock ratio (W:R). The duration of 4 years is obtained by using a W:R of 50, which is a realistic ratio in moderately concentrated flows. This duration is consistent with the $\sim$11 years proposed by Fassett and Head (2005), using their discharge rate estimations on the fan, and the 20–40 years of Schon *et al.* (2012) based on scroll bar migration.

More in-depth modeling of the discharge rates using the channels at the entrance of Jezero crater has been done by Salese *et al.* (2019a, 2020). Results give durations of the hydrological activity leading to the formation of the fan-delta in hundreds of years (90–550 years) with varying parameters. Even this duration is still a minimum given the possible intermittency in floods; it corresponds to the overall time of the hydrological activity needed to form such fan-deltas, and it thus has important implications for climatic constraints. This relatively short duration at geological scale is consistent with the possible duration of late-stage fluvial episodes observed throughout the planet (Kite *et al.*, 2019 and references therein) but it does not rule out the possibility that Jezero fan-delta formations correspond to the last gasp of the Late Noachian optimum.

5.2. Implications of the Jezero crater as a landing site for the Mars 2020 Perseverance rover

This study highlights several important conclusions relevant to Mars 2020's exploration and future sampling of deposits within the Jezero crater. The observed late-stage episode, potentially Hesperian, and the high discharge rates of the channels immediately upstream the main fan-delta question the exobiological relevance of the Jezero crater with regard to Early Mars climate. A late-stage, short-duration lake could have been permissive of the incipience and development of any microbial life.

The same argument might be poised against the probability that the subaqueous deposits that are the most accessible by the rover may be dominated by Hesperian sedimentary rocks, and thus they are potentially less relevant to exobiological studies than those formed earlier (McLennan *et al.*, 2011). Indeed, the specific evolution of Mars as a planet suggests that the best time interval for the search for biosignatures would be represented by early to mid-Noachian rocks, when clays were thought to be forming (Summons *et al.*, 2011). However, aqueous activity existed a while before this ultimate episode and this may have already started a biologically active environment, incorporated and fossilized *in situ* organics.

Besides the general favorable sedimentary context, the western Jezero fan sediments contain phyllosilicates in the form of iron–magnesium smectite clays and carbonates (Ehlmann *et al.*, 2008a). Abundant observational and experimental data show that many phyllosilicates, particularly smectites, are capable of preserving organic material due to strong absorption capacity, low reactivity, and low permeability when compacted (Meyers and Ishiwatari, 1995; Farmer and Des Marais, 1999). As a sedimentary sink, the Jezero crater lake represents a terminal receptor for both primary and transported organics, and Jezero crater clay-bearing deposits appear to be very appropriate biosignature repositories. The catchment west of Jezero crater includes a broad area with a diversity of volcanic-related rocks, including many locations with alteration minerals that have been interpreted to be of hydrothermal origin (*e.g.*, Mangold *et al.*, 2007; Mustard *et al.*, 2009; Goudge *et al.*, 2015). These locations could have been favorable to biological activity before the fan formation. Whatever the duration and age of the fan-delta, the layers at the bottom of the fan deposits (bottomsets) would have concentrated fine-grained materials that are favorable for organic materials, especially inside phyllosilicates that are favorable to their preservation.

In terms of depositional environment, the high channel discharges estimated, at least for the latest stages of activity, imply that deposits would be dominated by coarse-grained clastic deposits (coarse sandstones, conglomerates) without a good potential for biosignature preservation. Nevertheless, ancient organic molecules will be preserved only if buried in sediments, and long-term preservation will occur only if buried organics are shielded from oxidizing fluids.

The most beneficial influence of the limited-in-time, late depositional activity at Jezero crater certainly lies in the possibility that any potential organic matter, ''pelagic'' or transported in the Jezero crater, was probably buried rapidly, impeding chemical dissociation and thermal alteration of the organic molecules. Thus, one of the implications for exobiology of this study is that there may be a higher probability to find organics inside the Jezero crater sedimentary deposits that would have collected and concentrated previously formed organics in the finest-grain deposits (such as in bottomsets) rather than expecting organics formed during Jezero paleolake activity (with poor concentration expected), or organics preserved inside the coarser-grained locations of the delta deposits (topsets and inverted channels).

Lastly, several aspects of our work are testable from *in situ* or sample-returned data. The sampling of the grain size of fluvial channels of the delta would enable to reassess the calculations made in the work of Salese *et al.* (2019a, 2020), and thus, improve the estimations made for the paleolake activity duration. Another benefit of the coarse detrital component would be that the fan-delta would act as a sampling bag of most types of bedrock present upstream, in a widespread basin, including olivine/carbonate-rich rocks and clay-bearing altered basement (as discussed by Goudge *et al.*, 2015 and 2018), thus potentially enabling the identification of source rocks *in situ*. Samples returned from coarse sedimentary rocks could enable determination of their age and magmatic origin.

6. Conclusions

The morphometry of the fluvial valleys leading to the Jezero crater was studied to better understand the context and timing of the fluvial activity that led to the formation of the Jezero paleolake and depositional fans that were initially described by Fassett and Head (2005). Two fluvial valleys enter the Jezero crater, to its west (Neretva Vallis) and north, both forming depositional fans. Neretva Vallis is divisible into an upper section (130 km long) with significant erosion observed from the deep canyons (down to 400 m, 4 km wide) cutting into the basement plateau (53 km^3 of erosion), and a lower section (70 km long) with less erosion (<3 km^3) and immature valley development, pointing toward a different erosional style and a distinct period of activity.

The longitudinal and transversal topographic profiles of the western valley show that the degree of erosion reached in the upper part cannot account for the topography observed in the lower section and at the entrance into the Jezero crater. Our interpretation of these differences is that the main fluvial erosion occurred before the olivine-rich unit draping part of this region was deposited, and that a subsequent fluvial episode explains the lower valley morphometry, which is directly linked to the fan-delta inside the Jezero crater.

Crosscutting relationships and crater counts on the fan-delta have enabled us to constrain this episode to the Late Noachian or Hesperian. However, the deep upper valleys are consistent with typical Noachian fluvial activity on Mars; whereas the lower valley morphology present pristine channel landforms, high channel discharge rates, and a relatively short duration of formation of the main depositional fan (Salese *et al.*, 2019a, 2020), all of which are characteristics that are typically observed for late-stage processes (deltaic deposits, alluvial fans; Kite *et al.*, 2017). An Hesperian age should, therefore, be considered as a serious alternative to a Noachian age for the Jezero fan-deltas' formation. In contrast, crater counts conclude about an age that is strictly older than 3.2 Gy, thus discarding an Amazonian age for the fan-delta formation.

Considering the favorable depositional environment and mineralogy it affords, the western Jezero fan has retained much credence to ensure a substantial potential for preserving biosignatures and to maximize the science return from the robotic payload and samples. However, risks exist regarding the timing and duration of the paleolake activity, potentially postdating the optimum of fluvial activity and aqueous alteration on Mars in the Noachian. One of the implications for exobiology of this study is that there may be a higher probability of finding organics inside the Jezero crater sedimentary deposits that would have collected and concentrated previously formed organics in the finest-grain deposits (such as in bottomsets) rather than expecting organics formed during Jezero paleolake activity or organics preserved inside the coarser-grained locations of the delta deposits (topsets and inverted channels). Ground truth by the Perseverance rover will provide key information with which to validate or invalidate some of the interpretations made in this study. Nevertheless, our results should be considered when conducting a realistic set of analyses by the rover, as well as in the selection of samples of interest for a future mission of sample return (iMOST, 2019).

Acknowledgments

The authors thank G. Gulick, S. Holo, and M. Lapôtre for their insightful comments. They acknowledge discussions within the Mars 2020 Perseverance rover Science Team. The data (HRSC, CTX, HiRISE, MOLA) that support the findings of this study were obtained freely from the Planetary Data System (PDS) and are publicly available online at https://pds.nasa.gov/index.shtml. The authors wish to thank MRO and HRSC team for these data.

Author Disclosure Statement

No competing financial interests exist.

Funding Information

French authors are supported by the CNES (Centre National d'Etudes Spatiales), and Francesco Salese is supported by Marie Curie Individual Postdoctoral Fellowship (WET_MARS, Grant Agreement No. 795192).

References

Adeli, S., Hauber, E., Kleinhans, M., Le Deit, L., Platz, T., Fawdon, P., and Jaumann, R. (2016) Amazonian-aged fluvial system and associated ice-related features in Terra Cimmeria, Mars. *Icarus* 277:286–299.

Ansan, V. and Mangold, N. (2013) 3D Morphometry of valley networks on Mars from HRSC/MEX DEMs: implications for climatic evolution through time. *J Geophys Res* 118:1–22.

Baker, V.R. and Partridge, J.B. (1986) Small Martian valleys—pristine and degraded morphology. *J Geophys Res* 91(B3): 3561–3572.

Baker, V.R., Carr, M.H., Gulick, V.C., Williams, C.R., and Marley, M.S. (1992) Channels and valley networks. In *Mars*, edited by H.H. Kieffer, B.M. Jakosky, C.W. Snyder, and M. Matthews; University of Arizona Press, Tucson, pp 493–522.

Berlin, M.M. and Anderson, R.S. (2009) Steepened channels upstream of knickpoints: controls on relict landscape response. *J Geophys Res* 114:F03018.

Bramble, M.S., Mustard, J.F., and Salvatore, M.R. (2017) The geological history of Northeast Syrtis Major, Mars. *Icarus* 293:66–93.

Bursztyn, N., Pederson, J.L., Tressler, C., Mackley, R.D., and Mitchell, K.J. (2015) Rock strength along a fluvial transect of the Colorado Plateau—quantifying a fundamental control on geomorphology. *Earth Planet Sci Let* 429:90–100.

Carr, M.H. (1987) Water on Mars. *Nature* 326:30–35.

Carr, M.H. and Chuang, F. (1997) Martian drainage densities. *J Geophys Res-Planets* 102:9145–9152.

Charlton, R. (2007) *Fundamentals of Fluvial Geomorphology*. Taylor & Francis, Oxford, UK, p 280.

Craddock, R.A. and Howard, A.D. (2002) The case for rainfall on a warm, wet early Mars. *J Geophys Res* 107(E11): 5111.

Davis, S.N. and DeWiest, R.J.M. (1966) *Hydrogeology*. John Wiley, New York.

Di Achille, G., Ori, G.G., and Reiss, D. (2007) Evidence for late Hesperian lacustrine activity in Shalbatana Vallis, Mars. *J Geophys Res* 112:E07007.

Ehlmann, B.L. and Mustard, J.F. (2012) An in-situ record of major environmental transitions on early Mars at North Syrtis Major. *Geophys Res Let* 39:L11202.

Ehlmann, B.L., Mustard, J.F., Fassett, C.I., Schon, S.C., Head, J.W., III, Des Marais, D.J., Grant, J.A., and Murchie, S.L. (2008a) Clay minerals in delta deposits and organic preservation potential on Mars. *Nat Geosci* 1:355–358.

Ehlmann, B.L., Mustard, J.F., Murchie, S.L., Poulet, F., Bishop, J.L., Brown, A.J., Calvin, W.M., Clark, R.N., Des Marais, D.J., Milliken, R.E., Roach, L.H., Roush, T.L., Swayze, G.A., and Wray, J.J. (2008b) Orbital identification of carbonate-bearing rocks on Mars. *Science* 322:1828–1832.

Ehlmann, B.L., Mustard, J.F., Swayze, G.A., Clark, R.N., Bishop, J.L., Poulet, F., Des Marais, D.J., Roach, L.H., Milliken, R.E., Wray, J.J., Barnouilh-Jha, O., and Murchie, S.L. (2009) Identification of hydrated silicate minerals on Mars using MRO-CRISM: geologic context near Nili Fossae and implications for aqueous al-teration. *J Geophys Res* 114:E00D08.

El Maarry, M.R., Kodikara, J., Wijessoriya, S., Markiewicz, W.J., and Thomas, N. (2012) Desiccation mechanism for formation of giant polygons on Earth and intermediate-sized polygons on Mars: results from a pre-fracture model. *Earth Planet Sci Lett* 323:19–26.

Farmer, J.D. and Des Marais, D.J. (1999) Exploring for a record of ancient Martian life. *J Geophys Res* 104:977–995.

Fassett, C.I. and Head, J.W. (2005) Fluvial sedimentary deposits on Mars: ancient deltas in a crater lake in the Nili Fossae region. *Geophys Res Lett* 32:L14201.

Fassett, C.I. and Head, J.W. (2008) The timing of martian valley network activity: con-straints from buffered crater counting. *Icarus* 195:61–89.

Forster, M.A. and Kelsey, H.M. (2012) Knickpoint and knickzone formation and propogation, South Fork Eel River, Northern California. *Geosphere* 8:403–416.

Goldspiel, J.M. and Squyres, S.W. (2000) Groundwater sapping and valley formation on Mars. *Icarus* 148:176–192.

Goudge, T.A., Mustard, J.F., Head, J.W., Fassett, C.I., and Wiseman, S.M. (2015) Assessing the mineralogy of the watershed and fan deposits of the Jezero crater pale-olake system, Mars. *J Geophys Res* 120:775–808.

Goudge, T.A., Milliken, R.A., Head, J.W., Mustard, J.F., and Fassett, C.I. (2017) Sedimentological evidence for a deltaic origin of the western fan deposit in Jezero crater, Mars and implications for future exploration. *Earth Planet Sci Lett* 458: 357–365.

Goudge, T.A., Mohrig, D., Cardenas, B.T., Hugues, C.M., and Fassett, C.I. (2018) Stratigraphy and plaohydrology of delta channel deposits, Jezero crater, Mars. *Icarus* 301:58–75.

Gulick, V.C. (1998) Magmatic intrusions and a hydrothermal origin for fluvial valleys on Mars. *J Geophys Res* 103:19365–19387.

Gulick, V.C. (2001) Origin of the valley networks on Mars: a hydrological perspective. *Geomorphology* 37:241–268.

Gulick, V.C. and Baker, V.R. (1990) Origin and evolution of valleys on Martian volcanoes. *J Geophys Res Solid Earth* 95 (B9):14325–14344.

Gwinner, K., Scholten, F., Preusker, F., Elgner, S., Roatsch, T., Spiegel, M., Schmidt, R., Oberst, J., Jaumann, R., and Heipke, C. (2010) Topography of Mars from global mapping by HRSC high-resolution digital terrain models and orthoimages: characteristics and performance. *Earth Planet Sci Lett* 294:506–519.

Hamilton, V.E. and Christensen, P.R. (2005) Evidence for extensive, olivine-rich bedrock on Mars. *Geology* 33:433–436.

Hargitai, H., Gulick, V., and Glines, N. (2017) Discontinuous drainage systems formed by precipitation and ground-water outflow in the Navua Valles and Southwest Hadriacus Mons regions, Mars. *Icarus* 294:172–200.

Hargitai, H., Gulick, V., and Glines, N. (2018) The geology of the Navua Valles region of Mars. *J Maps* 14:504–508.

Hargitai, H.I., Gulick, V.C., and Glines, N.H. (2019) Evolution of the Navua Valles region: implications for Mars' paleoclimatic history. *Icarus* 330:91–102.

Hartmann, W.K. and Neukum, G. (2001) Cratering chronology and the evolution of Mars. *Space Sci Rev* 96:165–194.

Hauber, E., Van Gasselt, S., Ivanov, B., Werner, S., Head, J.W., Neukum, G., Jaumann, R., Greeley, R., Mitchell, K.L., and Muller, P.; HRSC Co-Investigator Team. (2005) Discovery of a flank caldera and very young glacial activity at Hecates Tholus, Mars. *Nature* 434:356–358.

Hauber, E., Gwinner, K., Kleinhans, M., Reiss, D., di Achille, G., Ori, G.-G., Scholten, F., Marinangeli, L., Jaumann, R., and Neukum, G. (2009) Sedimentary deposits in Xanthe Terra: implications for the ancient climate on Mars. *Planet Space Sci* 57:944–957.

Hey, R.D. and Thorne, C.R. (1986) Stable channels with mobile gravel beds. *J Hydraul Eng* 112:671.

Hiesinger, H. and Head, J.W. (2004) The Syrtis Major volcanic province, Mars: synthesis from Mars Global Surveyor data. *J Geophys Res* 109:E01004.

Hoefen, T.M., Clark, R.N., Bandfield, J.L., Smith, M.D., Pearl, J.C., and Christensen, P.R. (2003) Discovery of olivine in the Nili Fossae region of Mars. *Science* 302:627–630.

Holo, S.J. and Kite, E.S. (2017) Incision of the Jezero crater outflow channel by fluvial sediment transport [abstract number

3007]. In *4th Conference on Early Mars*, Houston, TX, LPI contribution 2014.

Howard, A.D. (1986) Groundwater sapping on Mars and Earth. Paper presented at *Proceedings and Field Guide, NASA Groundwater Sapping Conference*, edited by A.D. Howard, R.C. Kochel, and H.E. Holt, National Aeronautics and Space Administration, Flagstaff, AZ, pp vi–xiv.

Howard, A.D., Moore, J.M., and Irwin, R.P. (2005) An intense terminal epoch of widespread fluvial activity on early Mars: 1.Valley network incision and associated deposits. *J Geophys Res* 110:E12S14.

International Mars Sample Return Objectives and Samples Team (iMOST), Beaty, D.W., Grady, M.M., McSween, H.Y., Sefton-Nash, E., Carrier, B.L., Altieri, F., Amelin, Y., Ammannito, E., Anand, M., Benning, L.G., Bishop, J.L., Borg, L.E., Boucher, D., Brucato, J.R., Busemann, H., Campbell, K.A., Czaja, A.D., Debaille, V., Des Marais, D.J., Dixon, M., Ehlmann, B.L., Farmer, J.D., Fernandez-Remolar, D.C., Filiberto, J., Fogarty, J., Glavin, D.P., Goreva, Y.S., Hallis, L.J., Harrington, A.D., Hausrath, E.M., Herd, C.D.K., Horgan, B., Humanyun, M., Kleine, T., Kleinhenz, J., Mackelprang, R., Mangold, N., Mayhew, L.E., McCoy, J.T., McCubbin, F.M., McLennan, S.M., Moser, D.E., Moynier, F., Mustard, J.F., Niles, P.B., Ori, G.G., Raulin, F., Rettberg, P., Rucker, M.A., Schmitz, N., Schwenzer, S.P., Sephton, M.A., Shaheen, R., Sharp, Z.D., Schuster, D.L., Siljestrom, S., Smith, C.L., Spry, J.A., Steele, A., Swindle, T.D., Ten Kate, I.L., Tosca, N.J., Usui, T., Van Kranendonk, M.J., Wadhwa, M., Weiss, B.P., Werner, S.C., Westall, F., Wheeler, R.M., Zipfel, J., and Zorzano, M.P. (2019) The potential science and engineering value of samples delivered to Earth by Mars sample return. *Meteorit Planet Sci* 54(S1):S3–S152.

Irwin, R.P., Craddock, R.A., and Howard, A.D. (2005) Interior channels in Martian valley networks: discharge and runoff productions. *Geology* 33:489–492.

Irwin, R.P., Howard, A.D., and Craddock, R.A. (2008) Fluvial valley networks on Mars. In *River Confluences, Tributaries and the Fluvial Network*, edited by S.P. Rice, A.G. Roy, and B.L. Rhoads, Wiley & Sons, New York, pp 419–451.

Johnson, K.N. (2016) Causes and Consequences of Meandering in Bedrock Rivers: How interactions between rock properties and environmental conditions shape landscapes. Ph.D. Thesis, UC Santa Cruz.

Jones, A.P., McEwen, A.S., Tornabene, L.L., Baker, V.R., Melosh, H.J., and Berman, D.C. (2011) A geomorphic analysis of Hale crater, Mars: the effects of impact into ice-rich crust. *Icarus* 211:259–272.

Kirk, R.L., Howington-Kraus, E., Rosiek, M.R., Anderson, J.A., Archinal, B.A., Becker, K.J., Cook, D.A., Galuszka, D.M., Geissler, P.E., Hare, T.M., Holmberg, I.M., Keszthelyi, L.P., Redding, B.L., Delamere, W.A., Gallagher, D., Chapel, J.D., Eliason, E.M., King, R., and McEwen, A.S. (2008) Ultrahigh resolution topographic mapping of Mars with MRO HiRISE stereo images: meter-scale slopes of candidate Phoenix landing sites. *J Geophys Res* 113(E3):E00A24.

Kite, E.S., Sneed, J.S. Mayer, D.P., and Wilson, S.A. (2017) Persistent or repeated surface habitability on Mars during the Late Hesperian—Amazonian. *Geophys Res Lett* 44:3991–3999.

Kite, E.S., Mayer, D.P., Wilson, S.A., Davis, J.M., Lucas, A.S., and Stucky de Quay, G. (2019) Persistence of intense, climate-driven runoff late in Mars history. *Sci Adv* 5: eaav7710.

Kleinhans, M.G. (2005) Flow discharge and sediment transport models for estimating a minimum timescale of hydrological activity and channel and delta formation on Mars. *J Geophys Res* 110:E12003.

Kleinhans, M.G., van de Kasteele, H.E., and Hauber, E. (2010) Palaeoflow reconstruction from fan delta morphology on Mars. *Earth Planet Sci Lett* 294:378–392.

Knighton, D. (1998) *Fluvial Forms and Processes*. Oxford University Press, Oxford, UK, p 384.

Komar, P.D. (1979) Comparisons of the hydraulics of water flows in Martian outflow channels with flows of similar scale on Earth. *Icarus* 37:156–181.

Konsoer, K.M., LeRoy, J., Burr, D., Parker, G., Jacobsen, R., and Turnel, D. (2018) Channel slope adjustment in reduced gravity environments and implications for Martian channels. *Geology* 46:183–186.

Kremer, C.H., Mustard, J.F., and Bramble, M.S. (2019) A widespread olivine-rich ash deposit on Mars. *Geology* 47: 677–681.

Laity, J.E. and Malin, M.C. (1985) Sapping processes and the development of theater-headed valley networks on the colorado Plateau. *Geol Soc Am Bull* 96:203–217.

Lamb, M.P., Dietrich, W.E., Aciego, S.M., Depaolo, D.J., and Manga, M. (2008) Formation of Box Canyon, Idaho, by megaflood: implications for seepage erosion on Earth and Mars. *Science* 320:1067–1070.

Lapotre, M.G.A. and Lamb, M.P. (2018) Substrate controls on valley formation by groundwater on Earth and Mars. *Geology* 46:531–534.

Loget, N. and Vand Den Driessche, J. (2009) Wave train model for knickpoint migration. *Geomorphology* 106, 3–4:376–382.

MacDonald, G.A., Abbott, A.T., and Peterson, F.L. (1983) *Volcanoes in the Sea: The Geology of Hawaii*. University of Hawaii Press, Honolulu, HI.

Malin, M.C. and Carr, M.H. (1999) Groundwater formation of Martian valleys. *Nature* 397:589–591.

Malin, M.C., Bell, J.F., III, Cantor, B.A., Caplinger, M.A., Calvin, W.M., Clancy, R.T., Edgett, K.S.L., Edwards, Haberle, R.M., James, P.B., Lee, S.W., Ravine, M.A., Thomas, P.C., and Wolff, M.J. (2007) Context Camera Investigation on board the Mars Reconnaissance Orbiter. *J Geophys Res* 112:E05S04.

Mandon, L., Quantin-Nataf, C., Thollot, P., Mangold, N., Lozac'h, L., Dromart, G., Beck, P., Dehouck, E., Breton, S., Millot, C., and Volat, M. (2020) Refining the age, emplacement and alteration scenarios of the olivine-rich unit in the Nili Fossae region, Mars. *Icarus* 336:113436.

Mangold, N. (2012) Fluvial landforms on fresh ejecta craters. *Planet Space Sci* 62:69–85.

Mangold, N. and Howard, A.D. (2013) Outflow channels with deltaic deposits in Ismenius Lacus, Mars. *Icarus* 226:385–401.

Mangold, N., Poulet, F., Mustard, J., Bibring, J.-P., Gondet, B., Langevin, Y., Ansan, V., Masson, Ph., Fassett, C., Head, J.W., Hoffmann, H., and Neukum, G. (2007) Mineralogy of the Nili Fossae region with OMEGA/Mars Express data: 2. Aqueous alteration of the crust. *J Geophys Res* 112:E08S04.

Mangold, N., Ansan, V., Masson, Ph., Quantin, C., and Neukum, G. (2008) Geomorphic study of fluvial landforms on the northern Valles Marineris plateau, Mars. *J Geophys Res* 113: E08009.

Mangold, N., Adeli, S., Conway, S., Ansan, V., and Langlais B. (2012a) A chronology of early Mars climatic evolution from impact crater degradation. *J Geophys Res* 117:E04003.

Mangold, N., Kite, E.S., Kleinhans, M., Newsom, H., Ansan, V., Hauber, E., Kraal, E., Quantin-Nataf, C., and Tanaka, K. (2012b) The origin and timing of fluvial activity at the Eberswalde crater, Mars. *Icarus* 220:530–551.

McEwen, A.S., Eliason, E.M, Bergstrom, J.W., Bridges, N.T., Hansen, C.J., Delamere, W.A., Grant, J.A., Gulick, V.C., Herkenhoff, K.E., Keszthleyi, L., Kirk, R., Mellon, M.T., Squyres, S.W., Thomas, N., and Weitz, C.M. (2007) Mars reconnaissance orbiter's high resolution imaging science experiment (HiRISE). *J Geophys Res* 112:E05S02.

McLennan, S.M., Sephton, M.A., Allen, C., Allwood, A.C., Barbieri, R., Beaty, D.W., Boston, P., Carr, M., Grady, M., Grant, J., Heber, V.S., Herd, C.D.K., Hofmann, B., King, P., Mangold, N., Ori, G.G., Rossi, A.P., Raulin, F., Ruff, S.W., Sherwood Lollar, B., Symes, S., and Wilson, M.G. (2011) Planning for Mars returned sample science: final report of the MSR End-to-End International Science Analysis Group (E2E-iSAG). *Astrobiology* 12:175–230.

Meyers, P.A. and Ishiwatari, R. (1995) Organic matter accumulation records in lake sediments. In *Physics and Chemistry of Lakes*, edited by A. Lerman, D.M. Imboden, and J.R. Gat, Springer-Verlag, Berlin; pp 279–328.

Michael, G.G. and Neukum, G. (2010) Planetary surface dating from crater size-frequency distribution measurements: partial resurfacing events and statistical age uncertainty. *Earth Planet Sci Lett* 294:223–229.

Montgomery, D.R. and Gran, K.B. (2001) Downstream variations in the width of bedrock channels. *Water Resour Res* 37: 1841–1846.

Mustard, J.F., Poulet, F., Head, J.W., Mangold, N., Bibring, J.-P., Pelkey, S.M., Fassett, C.I., Langevin, Y., and Neukum G. (2007) Mineralogy of the Nili Fossae region with OMEGA/Mars Express data: 2. Ancient impact melt in the Isidis Basin and implications for the transition from the Noachian to Hesperian. *J Geophys Res* 112:E08S03.

Mustard, J.F., Murchie, S.L., Pelkey, S.M., Ehlmann, B.L., Milliken, R.E., Grant, J.A., Bibring, J.-P., Poulet, F., Bishop, J., Noe Dobrea, E., Roach, L., Seelos, F., Arvidson, R.E., Wiseman, S., Green, R., Hash, C., Humm, D., Malaret, E., McGovern, J.A., Seelos, K., Clancy, T., Clark, R., Des Marais, D., Izenberg, N., Knudson, A., Langevin, Y., Martin, T., McGuire, P., Morris, R., Robinson, M., Roush, T., Smith, M., Swayze, G., Taylor, H., Titus, T., and Wolff, M. (2008) Hydrated silicate minerals on Mars observed by the Mars Reconnaissance Orbiter CRISM instrument. *Nature* 454:305–309.

Mustard, J.F., Ehlmann, B.L., Murchie, S.L., Poulet, F., Mangold, N., Head, J.W., Bibring, J.-P., and Roach, L.H. (2009) Composition, mineralogy, and stratigraphy of Noachian crust around the Isidis basin. *J Geophys Res* 114: E00D12.

Neukum, G. and the HRSC team. (2004) HRSC: The high resolution stereo camera of Mars Express. *ESA* SP1240: 17–35.

Osterkamp, W.R. and Hedman, E.R. (1982) Perennial-streamflow characteristics related to channel geometry and sediment in Missouri River basin. *US Geological Survey Professional Paper* 1242.

Pieri, D.C. (1980) Martian valleys: morphology, distribution, age, and origin. *Science* 210:895–897.

Poulet, F., Bibring, J.-P., Mustard, J.F., Gendrin, A., Mangold, N., Langevin, Y., Arvidson, R.E., Gondet, B., and Gomez, C. (2005) Phyllosilicates on Mars and implications for early Martian climate. *Nature* 438:623–627.

Quantin, C., Allemand, P., Mangold, N., Dromart, G., and Delacourt, C. (2005) Fluvial and lacustrine activity on layered deposits in Melas Chasma, Valles Marineris, Mars. *J Geophys Res* 110:E12S19.

Quantin-Nataf, C., Craddock, R.A., Dubuffet, F., Lozac'h, L., and Martinot, M. (2019) Decline of crater obliteration rates during early martian history. *Icarus* 317:427–433.

Reading, H.G., editor. (1996) *Sedimentary Environments: Processes, Facies and Stratigraphy*, 3rd ed., Blackwell Science, Boston, MA, p 688.

Roda, M., Kleinhans, M.G., Zegers, T.E., and Oosthoek, J.H. (2014) Catastrophic ice lake collapse in Aram Chaos, Mars. *Icarus* 236:104–121.

Rogers, A.D., Warner, N.H., Golombek, M.P., Head, J.W., III, and Cowart, J.C. (2018) Areally extensive surface bedrock exposures on Mars: many are clastic rocks, not lavas. *Geophys Res Lett* 45:1767–1777.

Rust, B.R. (1978) A classification of alluvial channel systems. Canadian Society of Petroleum Geologists. *Memoir* 5:187–198.

Salese, F., Di Achille, G., Neesemann, A., Ori, G.G., and Hauber, E. (2016) Hydrological and sedimentary analyses of well-preserved paleofluvial-paleolacustrine systems at Moa Valles, Mars. *J Geophys Res Planets* 121:194–232.

Salese, F., Mangold, N., Kleinhans, M.G., de Haas, T., Ansan, V., and Dromart, G. (2019a) Estimated minimum lifespan of the Jezero crater delta, Mars. In *50th Lunar and Planetary Science Conference*, Houston, TX, LPI contribution 2132.

Salese, F., Pondrelli, M., Neeseman, A., Schmidt, G., and Ori, G.G. (2019b) Geological evidence of planet-wide groundwater system on Mars. *J Geophys Res Planets* 124: 374–395.

Salese, F., Kleinhans, M.G., Mangold, N., Ansan, V., McMahon, W., de Haas, T., and Dromart, G. (2020) Estimated minimum lifespan of the Jezero fluvial delta (Mars). *Astrobiology* 20:977–993.

Salvatore, M.R., Goudge, T.A., Bramble, M.S., Edwards, C.S., Bandfield, J.L., Amador, E.S., Mustard, J.F., and Christensen, P.R. (2018) Bulk mineralogy of the NE syrtis and Jezero crater regions of Mars derived through thermal infrared spectral analyses. *Icarus* 301:76–96.

Schon, S.C., Head, J.W., and Fassett, C.I. (2012) An overfilled lacustrine system and progra-dational delta in Jezero crater, Mars: implications for Noachian climate. *Planet Space Sci* 67:28–45.

Segura, T.L., Toon, O.B., and Colaprete, A. (2008) Modeling the environmental effects of moderate-sized impacts on Mars. *J Geophys Res* 113:E11007.

Shahrzad, S., Kinch, K.M., Goudge, T.A., Fassett, C.I., Needham, D.H., Quantin-Nataf, C., and Knudsen, C.P. (2019) Crater statistics on the dark-toned, mafic-floor unit in Jezero crater, Mars. *Geophys Res Let* 46:2408–2416.

Silberman, E., Carter, R., Einstein, H., Hinds, J., and Powell, R. (1963) Friction factors in open channels. *J Hydraul Eng* 89: 97–143.

Smith, D.E., Zuber, M.T., Frey, H.V., Garvin, J.B., Head, J.W., Muhleman, D.O., Pettengill, G.H., Phillips, R.J., Solomon, S.C., Zwally, H.J., Banerdt, W.B., Duxbury, T.C., Golombek, M.P., Lemoine, F.G., Neumann, G.A., Rowlands, D.D., Aharonson, O., Ford, P.G., Ivanov, A.B., Johnson, C.L., McGovern, P.J., Abshire, J.B., Afzal, R.S., and Sun, X. (2001) Mars Orbiter Laser Altimeter: experiment summary after the first year of global mapping of Mars. *J Geophys Res* 106:23,689–23,722.

Summons, R.E., Amend, J.P., Bish, D., Buick, R., Cody, G.D., Des Marais, D.J., Dromart, G., Eigenbrode, J.L., Knoll, A.H., and Sumner, D.Y. (2011) Preservation of martian organic and environmental records: final report of the Mars biosignature working group. *Astrobiology* 11:157–181.

Tanaka, K.L. (1982) A new time-saving crater-count technique with application to narrow features. In *NASA Technical Memorandum*, TM-85127, pp 123–125

Tarnas, J.D., Mustard, J.F., Lin, H., Goudge, T.A., Amador, E.S., Bramble, M.S., Kremer, C.H., Zhang, X., Itoh, Y., and Parente, M. (2019) Orbital identification of hydrated silica in Jezero crater, Mars. *Geophys Res Lett* 46:12771–12782.

Valla, P., Van Der Beek, P.A., and Lague, D. (2010) Fluvial incision into bedrock: insights from morphometric analysis and numerical modeling of gorges incising glacial hanging valleys (Western Alps, France). *J Geophys Res Am Geophys Union* 115:F02010.

Vaz, D.A., Di Achille, G., Hynek, B.M., Nelson, W., and Williams, R.E. (2018) Global morphometric survey of Martian deltaic deposits: methods and validation. In *49th Lunar and Planetary Science Conference*, Houston, TX, #2083.

Willett, S.D., Mc Coy, S.W., and Beeson, H.W. (2018) Transience of the North American High Plains landscape and its impact on surface water. *Nature* 561:528–532.

Williams, R.M.E., Grotzinger, J.P., Dietrich, W.E., Gupta, S., Sumner, D.Y., Wiens, R.C., Mangold, N., Malin, M.C., Edgett, K.S., Maurice, S., Forni, O., Gasnault, O., Ollila, A., Newsom, H.E., Dromart, G., Palucis, M.C., Yingst, R.A., Anderson, R.B., Herkenhoff, K.E., Le Mouélic, S., Goetz, W., Madsen, M.B., Koefoed, A., Jensen, J.K., Bridges, J.C., Schwenzer, S.P., Lewis, K.W., Stack, K.M., Rubin, D., Kah, L.C., Bell III, J.F., Farmer, J.D., Sullivan, R., Van Beek, T., Blaney, D.L., Pariser, O., and Deen, R.G., MSL Science Team. (2013) Martian fluvial conglomerates at Gale Crater. *Science* 340:1068–1072. DOI: 10.1126/science.1237317.

Wilson, L., Ghatan, G.J., Head, J.W., III, and Mitchell, K.L. (2004) Mars outflow channels: a reappraisal of the estimation of water flow velocities from water depths, regional slopes, and channel floor properties. *J Geophys Res* 109: E09003.

Address correspondence to:
Nicolas Mangold
Laboratoire Planétologie et Géodynamique
UMR6112 CNRS
Faculté des Sciences
Université de Nantes
Nantes 44322
France

E-mail: nicolas.mangold@univ-nantes.fr

Submitted 26 June 2019
Accepted 16 April 2020
Associate Editor: Jack Mustard

Abbreviations Used

CTX = Context Camera
DEMs = digital elevation models
HRSC = High Resolution Stereo Camera
HiRISE = High Resolution Imaging Science Experiment
MOLA = Mars Observer Laser Altimeter
SV = small valleys